

# Structured learning of metric ensembles with application to person re-identification

Sakrapee Paisitkriangkrai<sup>a</sup>, Lin Wu<sup>a,b</sup>, Chunhua Shen<sup>a,b,\*</sup>, Anton van den Hengel<sup>a,b</sup>

<sup>a</sup>*School of Computer Science, The University of Adelaide, Australia*

<sup>b</sup>*Australian Centre for Robotic Vision, Australia*

## Abstract

Matching individuals across non-overlapping camera networks, known as person re-identification, is a fundamentally challenging problem due to the large visual appearance changes caused by variations of viewpoints, lighting, and occlusion. Approaches in literature can be categorized into two streams: The first stream is to develop reliable features against realistic conditions by combining several visual features in a pre-defined way; the second stream is to learn a metric from training data to ensure strong inter-class differences and intra-class similarities. However, seeking an optimal combination of visual features which is generic yet adaptive to different benchmarks is a unsolved problem, and metric learning models easily get over-fitted due to the scarcity of training data in person re-identification. In this paper, we propose two effective structured learning based approaches which explore the adaptive effects of visual features in recognizing persons in different benchmark data sets. Our framework is built on the basis of multiple low-level visual features with an optimal ensemble of their metrics. We formulate two optimization algorithms, CMC<sup>triplet</sup> and CMC<sup>top</sup>, which directly optimize evaluation measures commonly used in person re-identification, also known as the Cumulative Matching Characteristic (CMC) curve. The more standard CMC<sup>triplet</sup> formulation works on the triplet information by maximizing the relative distance between a matched pair and a mismatched pair in each triplet unit. The CMC<sup>top</sup> formulation, modeled on a structured learning of maximizing the correct identification among top candidates, is demonstrated to be more beneficial to person re-identification by directly optimizing an objective closer to the actual testing criteria. The combination of these factors leads to a person re-identification system which outperforms most existing algorithms. More importantly, we advance state-of-the-art results by improving the rank-1 recognition rates from 40% to 61% on the iLIDS benchmark, 16% to 22% on the PRID2011 benchmark, 43% to 50% on the VIPeR benchmark, 34% to 55% on the CUHK01 benchmark and 21% to 68% on the CUHK03 benchmark.

**Keywords:** Person re-identification, Learning to rank, Metric ensembles, Structured learning.

## 1. Introduction

The task of person re-identification (re-id) is to match pedestrian images observed from multiple disjoint cameras. An automated re-id system could save a lot of human labour in exhaustively searching for a person of interest from a large amount of video sequences, and it serves a way of maintaining identity information about targets in multiple views over potentially long periods of time. Despite extensive research efforts [10, 36, 51, 54, 46, 50, 33, 22, 49], person re-id is still a very challenging task due to (a) large variation in visual appearance (person's appearance often undergoes large variations across different camera views); (b) significant changes in human poses at the time the image was captured; (c) large amount of illumination changes, background clutter and occlusions; d) relatively low resolution and the different placement of the cameras. Moreover, the problem becomes increasingly difficult when persons share similar appearance, e.g., people wearing similar clothing style with similar color.

To address these challenges, existing research has concentrated on the development of sophisticated and robust features

to describe visual appearance under significant changes. Most of them use appearance-based features that are viewpoint invariant such as color and texture descriptors [7, 10, 13, 41]. However, the system that relies heavily on one specific type of visual cues, e.g., color, texture or shape, would not be practical and powerful enough to discriminate individuals with similar visual appearance. Some studies have tried to address the above problem by seeking a combination of robust and distinctive feature representation of person's appearance, ranging from color histogram [13], spatial co-occurrence representation [41], LBP [46], to color SIFT [50]. The basic idea of exploiting multiple visual features is to build an ensemble of metrics (distance functions), in which each distance function is learned using a single feature and the final distance is calculated from a weighted sum of these distance functions [7, 46, 50]. These works often pre-define distance weights, which need to be re-estimated beforehand for different data sets. However, such a pre-defined principle has some drawbacks.

- Different real-world re-id scenarios can have very different characteristics, e.g., variation in view angle, lighting and occlusion. Simply combining multiple distance functions using pre-determined weights may be undesirable as highly discriminative features in one environment might become irrelevant in another environment.

\*Corresponding author.

Email address: chhshen@gmail.com (Chunhua Shen)

- The effectiveness of distance learning heavily relies on the quality of the feature selected, and such selection requires some domain knowledge and expertise.
- Given that certain features are determined to be more reliable than others under a certain condition, applying a standard distance measure for each individual match is undesirable as it treats all features equally without differentiation on features.

In these ends, it necessarily demands a principled approach that is able to automatically select and learn weights for diverse metrics, meanwhile generic yet adaptive to different scenarios.

Person re-identification problem can also be cast as a learning problem in which either metrics or discriminative models are learned [4, 5, 18, 19, 44, 45, 46, 22, 43, 27, 52], which typically learn a distance measure by minimizing intraclass distance and maximizing interclass distance simultaneously. Thereby, they require sufficient labeled training data from each class<sup>1</sup> and most of them also require new training data when camera settings change. Nonetheless, in person re-id benchmark, available training data is relatively scarce, and thus inherently under-sampled for building a representative class distribution. This intrinsic characteristic of person re-id problem makes metric learning pipelines easily overfitted and unable to be applicable in small image sets.

To combat above difficulties simultaneously, in this paper, we introduce two structured learning based approaches to person re-id by learning weights of distance functions for low-level features. The first approach,  $\text{CMC}^{\text{triplet}}$ , optimizes the relative distance using the triplet units, each of which contains three person images, i.e., one person with a matched reference and a mismatched reference. Treating these triplet units as input, we formulate a large margin framework with triplet loss where the relative distance between the matched pair and the mismatched pair tends to be maximized. An illustration of  $\text{CMC}^{\text{triplet}}$  is shown in Fig. 1. This triplet based model is more natural for person re-id mainly because the intra-class and inter-class variation may vary significantly for different classes, making it inappropriate to require the distance between a matched/mismatched pair to fall within an absolute range [52]. Also, training images in person re-id are relatively scarce, whereas the triplet-based training model is to make comparison between any two data points rather than comparison between any data distribution boundaries or among clusters of data. This thus alleviates the over-fitting problem in person re-id given undersampled data. The second approach,  $\text{CMC}^{\text{top}}$ , is developed to maximize the average rank- $k$  recognition rate, in which  $k$  is chosen to be small, e.g.,  $k < 10$ . Setting the value of  $k$  to be small is crucial for many real-world applications since most surveillance operators typically inspect only the first ten or twenty items retrieved. Thus, we directly optimize the testing performance measure commonly used in CMC curve, i.e., the recognition rate at rank- $k$  by using structured learning.

The main contributions of this paper are three-fold:

- We propose two principled approaches,  $\text{CMC}^{\text{triplet}}$  and  $\text{CMC}^{\text{top}}$ , to build an ensemble of person re-id metrics. The standard approach  $\text{CMC}^{\text{triplet}}$  is developed based on triplet information, which more tolerant to large intra and inter-class variations, and alleviate the over-fitting problem in person re-id. The second approach of  $\text{CMC}^{\text{top}}$  directly optimizes an objective closer to the testing criteria by maximizing the correctness among top  $k$  matches using structured learning, which is empirically demonstrated to be more beneficial to improving recognition rates.
- We perform feature quantification by exploring the effects of diverse feature descriptors in recognizing persons in different benchmarks. An ensemble of metrics is formulated into a late fusion paradigm where a set of weights corresponding to visual features are automatically learnt. This late fusion scheme is empirically studied to be superior to various early fusions on visual features.
- Extensive experiments are carried out to demonstrate that by building an ensemble of person re-id metrics learned from different visual features, notable improvement on rank-1 recognition rate can be obtained. In addition, our ensemble approaches are highly flexible and can be combined with linear and non-linear metrics. For non-linear base metrics, we extend our approaches to be tractable and suitable to large-scale benchmark data sets by approximating the kernel learning.

## 2. Related Work

Typical person re-id systems consist of two major components: feature representation and metric learning. In feature representation, robust and discriminative features are constructed such that they can be used to describe the appearance of the same individual across different camera views under various changes and conditions [2, 3, 7, 10, 13, 41, 50, 51]. We briefly discuss some of these work below. More feature representations, which have been applied in person re-id, can be found in [11].

*Appearance based person re-identification.* Bazzani *et al.* represent a person by a global mean color histogram and recurrent local patterns through epitomic analysis [2]. Farenzena *et al.* propose the symmetry-driven accumulation of local features (**SDALF**) which exploits both symmetry and asymmetry, and represents each part of a person by a weighted color histogram, maximally stable color regions and texture information [7]. Gray and Tao introduce an ensemble of local features which combines three color channels with 19 texture channels [13]. Schwartz and Davis propose a discriminative appearance based model using partial least squares, in which multiple visual features: texture, gradient and color features are combined [38]. Li *et al.* propose a filter pairing neural network to learn visual features for the re-identification task [21]. Zhao *et al.*

<sup>1</sup>Images of each person in a training set form a class.

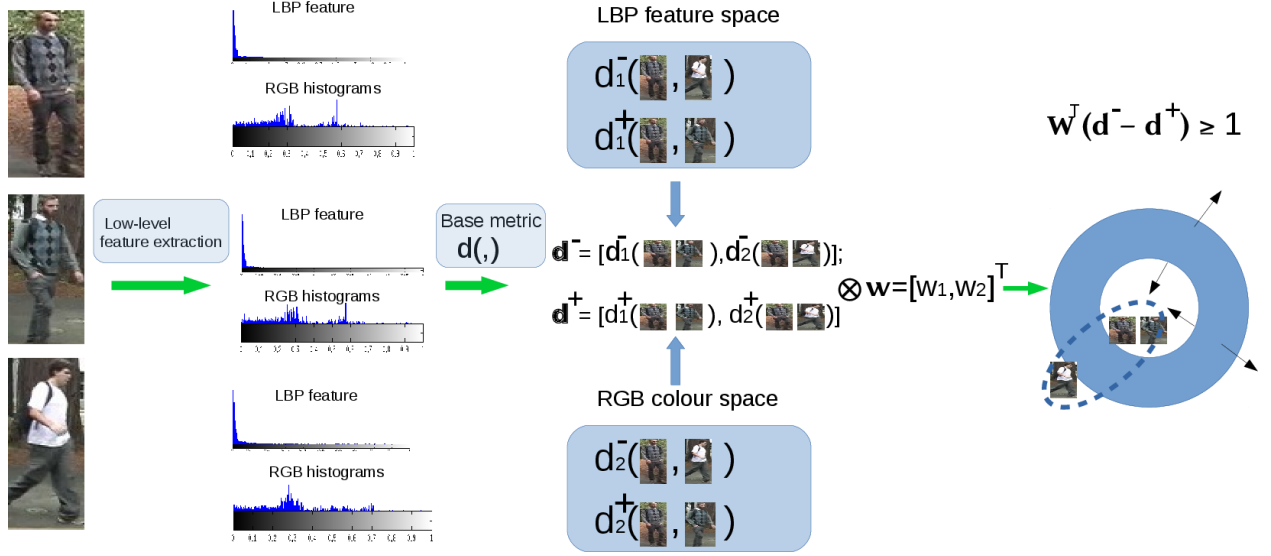


**Figure 1:** An illustration of our triplet-based framework. Given a set of triplets, our model is trained to fully exploit low-level features by adaptively learning weights for their distance functions, so as to maximize the relative distance between the matched pair and the mismatched pair for each triplet.

propose dcolorSIFT which combines SIFT features with color histogram. The authors combine dcolorSIFT with unsupervised salience learning to improve its discriminative power in person re-id [50] (**eSDC**), and further integrate both salience matching and patch matching into a unified RankSVM framework (**SalMatch** [49]). They also propose mid-level filters (**MidLevel**) for person re-identification by exploring the partial area under the ROC curve (pAUC) score [51]. Lisanti *et al.* [23] leverage low-level feature descriptors to approximate the appearance variants in order to discriminate individuals by using sparse linear reconstruction model (**ISR**).

*Metric learning based person re-identification:*. Another line to approach the problem of matching people across cameras is to essentially formalize person re-id as a supervised metric/distance learning where a projection matrix is sought out so that the projected Mahalanobis-like distance is small when feature vectors represent the same person and large otherwise. Along this line, a large number of metric learning and ranking algorithms have been proposed [4, 5, 33, 18, 19, 43, 44, 45, 46, 22, 27, 52]. We briefly review some of these algorithms. Interested readers should see [47]. Chopra *et al.* propose an algorithm to learn a similarity metric by training a convolutional network that maps input images into a target space such that the  $\ell_1$ -norm in the target space approximates the semantic distance in the image space[4]. Davis *et al.* presented information theoretic metric learning (**ITML**) which considered minimizing the differential relative entropy between two multivariate Gaussian for learning the Mahalanobis distance function [5]. Koestinger *et al.* propose the large-scale metric learning from equivalence constraint (**KISSME**) which considers a log likelihood ratio test of two Gaussian distributions [19]. Li *et al.* propose the learning of locally adaptive decision functions (**LADF**), which can be viewed as a joint model of a distance

metric and a locally adapted thresholding rule [22]. However, a drawback of this approach is that it scales poorly since its computational complexity is  $O(d^2)$  where  $d$  is the dimension of the feature vector. An alternative approach is to use a logistic function to approximate the hinge loss so that the global optimum still can be achieved by iteratively gradient search along the projection matrix as in Pairwise Constrained Component Analysis (**PCCA**) [27] and **PRDC** [52]. However, these methods are prone to over-fitting and can result in poor classification performance due to large variations among samples. We approach this problem by proposing a more generic algorithm which is developed based on triplet information so as to generate more constraints for distance learning, and thus mitigate the over-fitting issue. Prosser *et al.* use pairs of similar and dissimilar images and train the ensemble RankSVM such that the true match gets the highest rank [34]. However, the model of RankSVM needs to determine the weight between the margin function and the ranking error cost function, which is computationally costly. Weinberger *et al.* propose the large margin nearest neighbour (**LMNN**) algorithm to learn the Mahalanobis distance metric, which improves the k-nearest neighbour classification [43]. LMNN is later applied to person re-identification in [16]. Wu *et al.* applies the Metric Learning to Rank (**MLR**) method of [26] to person re-id [45]. Although a large number of existing algorithms have exploited state-of-the-art visual features and advanced metric learning algorithms, we observe that the best obtained overall performance on commonly evaluated person re-id benchmarks, e.g., iLIDS and VIPeR, is still far from the performance needed for most real-world surveillance applications. The goal of this paper is to show how one can carefully design a standard, generalized person re-id framework to achieve state-of-the-art results on person re-id testing data sets. Preliminary results of this work were published in [31].

### 3. Notations and Problem Definition

Bold lower-case letters, e.g.,  $\mathbf{w}$ , denote column vectors and bold upper-case letters, e.g.,  $\mathbf{P}$ , denote matrices. We assume that the provided training data is for the task of single-shot person re-identification, i.e., there exist only two images of the same person –one image taken from camera view A and another image taken from camera view B. We represent a set of training samples by  $\{(x_i, x_i^+)\}_{i=1}^m$  where  $x_i \in \mathbb{R}^D$  represents a training example from one camera (i.e., camera view A), and  $x_i^+$  is the corresponding image of the same person from a different camera (i.e., camera view B). Here  $m$  is the number of persons in the training data. From the given training data, we can generate a set of triplets for each sample  $x_i$  as  $\{(x_i, x_i^+, x_{i,j}^-)\}$  for  $i = 1, \dots, m$  and  $i \neq j$ . Here we introduce  $x_{i,j}^- \in X_i^-$  where  $X_i^-$  denotes a subset of images of persons with a different identity to  $x_i$  from camera view B. We also assume that there exist a set of distance functions  $d_t(\cdot, \cdot)$  which calculate the distance between two given inputs. Our goal is to learn a weighted distance function:  $d(\cdot, \cdot) = \sum_{t=1}^T w_t d_t(\cdot, \cdot)$ , such that the distance between  $x_i$  (taken from camera view A) and  $x_i^+$  (taken from camera view B) is smaller than the distance between  $x_i$  and any  $x_{i,j}^-$  (taken from camera view B). The better the distance function, the faster the cumulative matching characteristic (CMC) curve approaches one.

### 4. Our Approach

In this section, we propose two structured learning based approaches that can learn an ensemble of base metrics. We then discuss base metrics that will be used in our experiment as well as a strategy of approximating non-linear metric learning for the case of large-sized person re-id data set.

#### 4.1. Ensemble of base metrics

The most commonly used performance measure for evaluating person re-id is known as a cumulative matching characteristic (CMC) curve [12], which is analogous to the ROC curve in detection problems. The CMC curve represents results of an identification task by plotting the probability of correct identification (y-axis) against the number of candidates returned (x-axis). The faster the CMC curve approaches one, the better the person re-id algorithm. Since a better rank-1 recognition rate is often preferred [51], our aim is to improve the recognition rate among the  $k$  best candidates, e.g.,  $k < 20$ , which is crucial for many real-world surveillance applications. Note that, in practice, the system that achieves the best recognition rate when  $k$  is large (e.g.,  $k > 100$ ) is of little interest since most users inspect or consider only the first ten or twenty returned candidates. In this section, we propose two different approaches which learn an ensemble of base metrics (discussed in the next section). The first approach,  $\text{CMC}^{\text{triplet}}$ , aims at minimizing the number of returned list of candidates in order to achieve a perfect identification, i.e., minimizing  $k$  such that the rank- $k$  recognition rate is equal to one. The second approach,  $\text{CMC}^{\text{top}}$ , optimizes the probability that any of these  $k$  best matches are correct.

#### 4.2. Relative distance based approach ( $\text{CMC}^{\text{triplet}}$ )

In order to minimize  $k$  such that the rank- $k$  recognition rate is equal to 100%, we consider learning an ensemble of distance functions based on relative comparison of triplets [37]. Given a set of triplets  $\{(x_i, x_i^+, x_{i,j}^-)\}_{i,j}$ , in which  $x_i$  is taken from camera view A and  $\{x_i^+, x_{i,j}^-\}$  are taken from camera view B, the basic idea is to learn a distance function such that images of the same individual are closer than any images of different individuals, i.e.,  $x_i$  is closer to  $x_i^+$  than any  $x_{i,j}^-$ . For a triplet  $\{(x_i, x_i^+, x_{i,j}^-)\}_{i,j}$ , the following condition must hold  $d(x_i, x_{i,j}^-) > d(x_i, x_i^+)$ ,  $\forall j, i \neq j$ . Following the large margin framework with the hinge loss, the condition  $d(x_i, x_{i,j}^-) \geq 1 + d(x_i, x_i^+)$  should be satisfied. This condition means that the distance between two images of different individuals should be larger by at least a unit than the distance between two images of the same individual. Since the above condition cannot be satisfied by all triplets, we introduce a slack variable to enable soft margin. By generalizing the above idea to the entire training set, the primal problem that we want to optimize can be written as,

$$\begin{aligned} \min_{\mathbf{w}, \xi} \quad & \frac{1}{2} \|\mathbf{w}\|_2^2 + \nu \frac{1}{m(m-1)} \sum_{i=1}^m \sum_{j=1}^{m-1} \xi_{ij} \\ \text{s.t.} \quad & \mathbf{w}^\top (\mathbf{d}_j^- - \mathbf{d}_i^+) \geq 1 - \xi_{ij}, \forall \{i, j\}, i \neq j; \\ & \mathbf{w} \geq 0; \xi \geq 0. \end{aligned} \quad (1)$$

Here  $\nu > 0$  is the regularization parameter and  $\mathbf{d}_j^- = [d_1(x_i, x_{i,j}^-), \dots, d_t(x_i, x_{i,j}^-)]$ ,  $\mathbf{d}_i^+ = [d_1(x_i, x_i^+), \dots, d_t(x_i, x_i^+)]$  and  $\{d_1(\cdot, \cdot), \dots, d_t(\cdot, \cdot)\}$  represent a set of base metrics. Note that we introduce the regularization term  $\|\mathbf{w}\|_2^2$  to avoid the trivial solution of arbitrarily large  $\mathbf{w}$ . We point out here that any smooth convex loss function can also be applied. Suppose that  $\lambda(\cdot)$  is a smooth convex function defined in  $\mathbb{R}$  and  $\omega(\cdot)$  is any regularization function. The above optimization problem which enforces the relative comparison of the triplet can also be written as,

$$\begin{aligned} \min_{\mathbf{w}} \quad & \omega(\mathbf{w}) + \nu \sum_{\tau} \lambda(\rho_{\tau}) \\ \text{s.t.} \quad & \rho_{\tau} = \sum_t w_t d_t(x_i, x_{i,j}^-) - \sum_t w_t d_t(x_i, x_i^+), \forall \tau; \\ & \mathbf{w} \geq 0, \end{aligned} \quad (2)$$

where  $\tau$  being the triplet index set. In this paper, we consider the hinge loss but other convex loss functions [40] can be applied. Since the number of constraints in (1) is quadratic in the number of training examples, directly solving (1) using off-the-shelf optimization toolboxes can only solve problems with up to a few thousand training examples. In the following, we present an equivalent reformulation of (1), which can be efficiently solved in a linear runtime using cutting-plane algorithms. We first reformulate (1) by writing it as:

$$\begin{aligned} \min_{\mathbf{w}, \xi} \quad & \frac{1}{2} \|\mathbf{w}\|_2^2 + \nu \xi \\ \text{s.t.} \quad & \frac{1}{m(m-1)} \mathbf{w}^\top \left[ \sum_{i=1}^m \sum_{j=1}^{m-1} (\mathbf{d}_j^- - \mathbf{d}_i^+) \right] \geq 1 - \xi, \end{aligned} \quad (3)$$

$$\forall \{i, j\}, i \neq j; \mathbf{w} \geq 0; \xi \geq 0.$$

Note that the new formulation has a single slack variable. Later on in this section, we show how the cutting-plane method can be applied to solve (3).

#### 4.3. Top recognition at rank- $k$ (CMC<sup>top</sup>)

Our previous formulation assumes that, for any triplets, images belonging to the same individual should be closer than images belonging to different individuals. Our second formulation is motivated by the nature of the problem, in which person re-id users often browse only the first few retrieved matches. Hence we propose another approach, in which the objective is no longer to minimize  $k$  (the number of returned matches before achieving 100% recognition rate), but to maximize the correct identification among the top  $k$  best candidates. Built upon the structured learning framework [17, 29], we optimize the performance measure commonly used in the CMC curve (recognition rate at rank- $k$ ) using structured learning. The difference between our work and [29] is that [29] assumes training samples consist of  $m_+$  positive instances and  $m_-$  negative instances, while our work assumes that there are  $m$  individuals in camera view A and  $m$  individuals in camera view B. However there exists ranking in both works: [29] attempts to rank all positive samples before a subset of negative samples while our works attempt to rank a pair of the same individual above a pair of different individuals. Both also apply structure learning of [17] to solve the optimization problem. Given the training individual  $\mathbf{x}_i$  (from camera view A) and its correct match  $\mathbf{x}_i^+$  from camera view B, we can represent the relative ordering of all matching candidates in camera view B via a vector  $\mathbf{p} \in \mathbb{R}^{m'}$ , in which  $p_j$  is 0 if  $\mathbf{x}_i^+$  (from camera view B) is ranked *above*  $\mathbf{x}_{i,j}^-$  (from camera view B) and 1 if  $\mathbf{x}_i^+$  is ranked *below*  $\mathbf{x}_{i,j}^-$ . Here  $m'$  is the total number of individuals from camera view B who has a different identity to  $\mathbf{x}_i$ . Since there exists only one image of the same individual in the camera view B,  $m'$  is equal to  $m - 1$  where  $m$  is the total number of individuals in the training set. We generalize this idea to the entire training set and represent the relative ordering via a matrix  $\mathbf{P} \in \{0, 1\}^{m \times m'}$  as follows:

$$p_{ij} = \begin{cases} 0 & \text{if } \mathbf{x}_i^+ \text{ is ranked above } \mathbf{x}_{i,j}^- \\ 1 & \text{otherwise.} \end{cases} \quad (4)$$

The correct relative ordering of  $\mathbf{P}$  can be defined as  $\mathbf{P}^*$  where  $p_{ij}^* = 0, \forall i, j$ . The loss among the top  $k$  candidates can then be written as,

$$\Delta(\mathbf{P}^*, \mathbf{P}) = \frac{1}{m \cdot k} \sum_{i=1}^m \sum_{j=1}^k p_{i(j)}, \quad (5)$$

where  $(j)$  denotes the index of the retrieved candidates ranked in the  $j$ -th position among all top  $k$  best candidates. We define the joint feature map,  $\psi$ , of the form:

$$\psi(\mathbf{S}, \mathbf{P}) = \frac{1}{m \cdot k} \sum_{i=1}^m \sum_{j=1}^{m'} (1 - p_{ij})(\mathbf{d}_j^- - \mathbf{d}_i^+), \quad (6)$$

where  $\mathbf{S}$  represent a set of triplets generated from the training data,  $\mathbf{d}_j^- = [d_1(\mathbf{x}_i, \mathbf{x}_{i,j}^-), \dots, d_t(\mathbf{x}_i, \mathbf{x}_{i,j}^-)]$  and  $\mathbf{d}_i^+ = [d_1(\mathbf{x}_i, \mathbf{x}_i^+), \dots, d_t(\mathbf{x}_i, \mathbf{x}_i^+)]$ . The choice of  $\psi(\mathbf{S}, \mathbf{P})$  guarantees that the variable  $\mathbf{w}$ , which optimizes  $\mathbf{w}^\top \psi(\mathbf{S}, \mathbf{P})$ , will also produce the distance function  $d(\cdot, \cdot) = \sum_{t=1}^T w_t d_t(\cdot, \cdot)$  that achieves the optimal average recognition rate among the top  $k$  candidates. The above problem can be summarized as the following convex optimization problem:

$$\begin{aligned} \min_{\mathbf{w}, \xi} \quad & \frac{1}{2} \|\mathbf{w}\|_2^2 + \nu \xi \\ \text{s.t.} \quad & \mathbf{w}^\top (\psi(\mathbf{S}, \mathbf{P}^*) - \psi(\mathbf{S}, \mathbf{P})) \geq \Delta(\mathbf{P}^*, \mathbf{P}) - \xi, \end{aligned} \quad (7)$$

$\forall \mathbf{P}$  and  $\xi \geq 0$ . Here  $\mathbf{P}^*$  denote the correct relative ordering and  $\mathbf{P}$  denote any arbitrary orderings. Similar to CMC<sup>triplet</sup>, we use the cutting-plane method to solve (7).

##### 4.3.1. Cutting-plane optimization

In this section, we illustrate how the cutting-plane method can be used to solve both optimization problems: (3) and (7). The key idea of the cutting-plane is that a small subset of the constraints are sufficient to find an  $\epsilon$ -approximate solution to the original problem. The cutting-plane algorithm begins with an empty initial constraint set and iteratively adds the most violated constraint set. At each iteration, the algorithm computes the solution over the current working set. The algorithm then finds the most violated constraint and add it to the working set. The cutting-plane algorithm continues until no constraint is violated by more than  $\epsilon$ . Since the quadratic program is of constant size, the cutting-plane method converges in a constant number of iterations. We present our proposed CMC<sup>top</sup> in Algorithm 1.

The optimization problem for finding the most violated constraint (Algorithm 1, step ②) can be written as,

$$\begin{aligned} \bar{\mathbf{P}} &= \max_{\mathbf{P}} \Delta(\mathbf{P}^*, \mathbf{P}) - \mathbf{w}^\top (\psi(\mathbf{S}, \mathbf{P}^*) - \psi(\mathbf{S}, \mathbf{P})) \\ &= \max_{\mathbf{P}} \Delta(\mathbf{P}^*, \mathbf{P}) - \frac{1}{mk} \sum_{i,j} p_{ij} \mathbf{w}^\top (\mathbf{d}_j^- - \mathbf{d}_i^+) \\ &= \max_{\mathbf{P}} \sum_{i=1}^m \left( \sum_{j=1}^k p_{i(j)} (1 - \mathbf{w}^\top \mathbf{d}_{i(j)}^+) - \sum_{j=k+1}^{m'} p_{i(j)} \mathbf{w}^\top \mathbf{d}_{i(j)}^+ \right) \end{aligned} \quad (8)$$

where  $\mathbf{d}_{i(j)}^+ = \mathbf{d}_{i(j)}^- - \mathbf{d}_i^+$ . Since  $p_{ij}$  in (8) is independent, the solution to (8) can be solved by maximizing over each element  $p_{ij}$ . Hence  $\bar{\mathbf{P}}$  that most violates the constraint corresponds to,

$$\bar{p}_{i(j)} = \begin{cases} 1(\mathbf{w}^\top (\mathbf{d}_{i(j)}^- - \mathbf{d}_i^+) \leq 1), & \text{if } j \in \{1, \dots, k\} \\ 1(\mathbf{w}^\top (\mathbf{d}_{i(j)}^- - \mathbf{d}_i^+) \leq 0), & \text{otherwise.} \end{cases}$$

For CMC<sup>triplet</sup>, one replaces  $g(\mathbf{S}, \mathbf{P}, \mathbf{w})$  in Algorithm 1 with  $g(\mathbf{S}, \mathbf{w}) = 1 - \frac{1}{m(m-1)} \mathbf{w}^\top \left[ \sum_{i,j} (\mathbf{d}_j^- - \mathbf{d}_i^+) \right]$  and repeats the same procedure.

In this section we assume that the base metrics,  $\{d_1(\cdot, \cdot), \dots, d_t(\cdot, \cdot)\}$ , are provided. In the next section, we introduce two base metrics adopted in our proposed approaches.

---

**Algorithm 1** Cutting-plane algorithm for solving coefficients of base metrics (CMC<sup>top</sup>)

---

**Input:**

- 1) A set of base metrics of the same individual and different individuals  $\{d_i^+, d_j^-\}$ ;
- 2) The regularization parameter,  $\nu$ ;
- 3) The cutting-plane termination threshold,  $\epsilon$ ;

**Output:** The base metrics' coefficients  $\mathbf{w}$ ,

**Initialize:** The working set,  $C = \emptyset$ ;

$$g(S, P, \mathbf{w}) = \Delta(P^*, P) - \frac{1}{mk} \sum_{i,j} p_{ij} \mathbf{w}^\top (d_j^- - d_i^+);$$

**Repeat**

- ① Solve the primal problem using linear SVM,

$$\min_{\mathbf{w}, \xi} \frac{1}{2} \|\mathbf{w}\|_2^2 + \nu \xi \quad \text{s.t. } g(S, P, \mathbf{w}) \leq \xi, \forall P \in C;$$

- ② Compute the most violated constraint,

$$\bar{P} = \max_P g(S, P, \mathbf{w});$$

- ③  $C \leftarrow C \cup \{\bar{P}\}$ ;

**Until**  $g(S, P, \mathbf{w}) \leq \xi + \epsilon$ ;

---

#### 4.4. Base metrics

Metric learning can be divided into two categories: linear [5, 19, 43] and non-linear methods [4, 9, 18, 44, 46]. In the linear case, the goal is to learn a linear mapping by estimating a matrix  $\mathbf{M}$  such that the distance between images of the same individual,  $(\mathbf{x}_i - \mathbf{x}_i^+)^\top \mathbf{M} (\mathbf{x}_i - \mathbf{x}_i^+)$ , is less than the distance between images of different individuals,  $(\mathbf{x}_i - \mathbf{x}_{i,j}^-)^\top \mathbf{M} (\mathbf{x}_i - \mathbf{x}_{i,j}^-)$ . The linear method can be easily extended to learn non-linear mapping by kernelization [39]. The basic idea is to learn a linear mapping in the feature space of some non-linear function,  $\phi$ , such that the distance  $(\phi(\mathbf{x}_i) - \phi(\mathbf{x}_i^+))^\top \mathbf{M} (\phi(\mathbf{x}_i) - \phi(\mathbf{x}_i^+))$  is less than the distance  $(\phi(\mathbf{x}_i) - \phi(\mathbf{x}_{i,j}^-))^\top \mathbf{M} (\phi(\mathbf{x}_i) - \phi(\mathbf{x}_{i,j}^-))$ . By assuming that we can compute the kernel function,  $\kappa(\mathbf{x}, \mathbf{x}') = \phi(\mathbf{x})^\top \phi(\mathbf{x}')$ , we can efficiently learn  $\mathbf{M}$ . Although we introduce two metric learnings in this section, any metric learning algorithms can be applied here.

*Metric learning from equivalence constraints.* The basic idea of KISS metric learning (KISS ML) [19], is to learn the Mahalanobis distance by considering a log likelihood ratio test of two Gaussian distributions. The likelihood ratio test between dissimilar pairs and similar pairs can be written as,

$$r(\mathbf{x}_i, \mathbf{x}_j) = \log \frac{\frac{1}{c_d} \exp(-\frac{1}{2} \mathbf{x}_{ij}^\top \Sigma_{\mathcal{D}}^{-1} \mathbf{x}_{ij})}{\frac{1}{c_s} \exp(-\frac{1}{2} \mathbf{x}_{ij}^\top \Sigma_S^{-1} \mathbf{x}_{ij})}, \quad (9)$$

where  $\mathbf{x}_{ij} = \mathbf{x}_i - \mathbf{x}_j$ ,  $c_d = \sqrt{2\pi|\Sigma_{\mathcal{D}}|}$ ,  $c_s = \sqrt{2\pi|\Sigma_S|}$ ,  $\Sigma_{\mathcal{D}}$  and  $\Sigma_S$  are covariance matrices of dissimilar pairs and similar pairs, respectively. By taking log and discarding constant terms, (9) can be simplified as,

$$r(\mathbf{x}_i, \mathbf{x}_j) = (\mathbf{x}_i - \mathbf{x}_j)^\top (\Sigma_S^{-1} - \Sigma_{\mathcal{D}}^{-1}) (\mathbf{x}_i - \mathbf{x}_j), \quad (10)$$

Hence the Mahalanobis distance matrix  $\mathbf{M}$  can be written as  $\Sigma_S^{-1} - \Sigma_{\mathcal{D}}^{-1}$ . The authors of [19] clip the spectrum of  $\mathbf{M}$  by eigenanalysis to ensure  $\mathbf{M}$  is positive semi-definite. This simple algorithm has shown to perform surprisingly well on the person re-id problem [36, 21].

*Kernel-based metric learning.* There exist several non-linear extensions to metric learning. In this section, we introduce recently proposed kernel-based metric learning, known as kernel Local Fisher Discriminant Analysis (kLFDA) [46], which is a non-linear extension to the previously proposed LFDA [33] and has demonstrated the state-of-the-art performance on iLIDS, CAVIAR and 3DPeS data sets. The basic idea of kLFDA is to find a projection matrix  $\mathbf{M}$  which maximizes the between-class scatter matrix while minimizing the within-class scatter matrix using the Fisher discriminant objective. Similar to LFDA, the projection matrix can be estimated using generalized eigen-decomposition. Unlike LFDA, kLFDA represent the projection matrix with the data samples in the kernel space  $\phi(\cdot)$ .

#### 4.5. Approximate kernel learning for person re-id

By projecting data points into high-dimensional or even infinite-dimensional feature space, kernel methods are found very effective in person re-id application with strong generalization performance [46]. However, one limitation of kernel methods is their high computational cost, which is at least quadratic in the size of training samples, due to the calculation of kernel matrix. In the testing stage, the kernel similarity between any two identities cannot be computed directly but through their individual kernel similarities to training individuals. Thus, the time complexity of testing heavily depends on the number of training samples. For instance, in CUHK03 database, the number of individuals in the training is set to be 1260, which would cause inefficiency in testing. To avoid computing kernel matrix, a kernel learning problem is often approximated by a linear prediction problem where the kernel similarity between any two data points is approximated by their vector representations. Whilst both random Fourier features [35] and the Nyström method [6] have been successfully applied to efficient kernel learning, recent theoretical and empirical studies show that the Nyström method has a significantly better generalization performance than random Fourier features when there is a large eigengap of kernel matrix [48].

The Nyström method approximates the kernel matrix by randomly selecting a subset of training examples and computes a kernel matrix  $\widehat{K}$  for the random samples, leading to a data dependent vector representation. The additional error caused by the Nyström method in the generalization performance can be improved to be  $O(1/m)$  ( $m$  is the number of sampled training examples) when there is a large gap in the eigen-spectrum of the kernel matrix [48]. Thus, we employ an improved Nyström framework to approximate the kernel learning in large-sized person re-id databases. Specifically, given a collection of  $N$  training examples,  $X = \{(\mathbf{x}_1, y_1), \dots, (\mathbf{x}_N, y_N)\}$  where  $\mathbf{x}_i \in \mathcal{X} \subseteq \mathbb{R}^d$ ,  $y_i \in \mathcal{Y}$ . Let  $\kappa(\cdot, \cdot)$  be a kernel function,  $\mathcal{H}_k$  denote the endowed Reproducing Kernel Hilbert Space, and  $K = [\kappa(\mathbf{x}_i, \mathbf{x}_j)]_{N \times N}$  be the kernel matrix for the samples in  $X$ . The Nyström method approximate the full kernel matrix  $K$  by firstly sampling  $m$  examples, denoted by  $\hat{\mathbf{x}}_1, \dots, \hat{\mathbf{x}}_m$ , and then constructing a low rank matrix by  $\widehat{K}_r$  where  $r$  denotes the rank of  $\widehat{K} = [\kappa(\hat{\mathbf{x}}_i, \hat{\mathbf{x}}_j)]_{m \times m}$ . Thus, we can derive a vector representation of data by  $\mathbf{z}_n(\mathbf{x}) = \widehat{D}_r^{-1/2} \widehat{V}_r^\top (\kappa(\mathbf{x}, \hat{\mathbf{x}}_1), \dots, \kappa(\mathbf{x}, \hat{\mathbf{x}}_m))^\top$ , where  $\widehat{D}_r = \text{diag}(\hat{\lambda}_1, \dots, \hat{\lambda}_r)$ ,

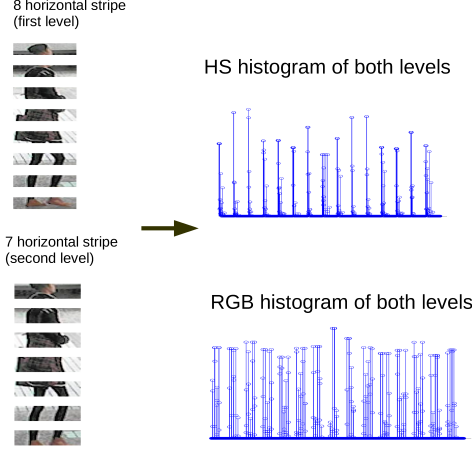


**Figure 2:** HS and RGB histograms extracted from overlapping stripes.

$\widehat{V}_r = (\widehat{v}_1, \dots, \widehat{v}_r)$ , and  $\widehat{\lambda}_i$  and  $\widehat{v}_i$  denote the eigenvalue and eigenvector of  $\widehat{K}_r$ , respectively. Given  $z_n(x)$ , we aim to learn a linear machine  $f(x) = w^T z_n(x)$  by solving the following optimization problem:

$$\min_{w \in \mathbb{R}^r} \frac{\lambda}{2} \|w\|_2^2 + \frac{1}{N} \sum_{i=1}^N l(w^T z_n(x_i), y_i). \quad (11)$$

In [48] Yang *et al.* construct an approximate functional space  $\mathcal{H}_a = \text{span}(\widehat{\phi}_1, \dots, \widehat{\phi}_r)$  where  $\widehat{\phi}_1, \dots, \widehat{\phi}_r$  are the first  $r$  normalized eigenfunctions of the operator  $L_m = \frac{1}{m} \sum_{i=1}^m \kappa(\widehat{x}_i, \cdot) f(\widehat{x}_i)$  and they subsequently obtain the following equivalent approximate kernel machine:

$$\min_{f \in \mathcal{H}_a} \frac{\lambda}{2} \|f\|_{\mathcal{H}_k}^2 + \frac{1}{N} \sum_{i=1}^N l(f(x_i), y_i).$$

According to both theoretical and empirical studies, the additional error caused by this approximation of the Nyström method is improved from  $O(1/\sqrt{m})$  to  $O(1/m)$  when there is a large gap between  $\lambda_r$  and  $\lambda_{r+1}$ . In our experimental study (section 5.8), the eigenvalue distributions of kernel matrices from different person re-id data sets are shown to demonstrate the existence of large eigengap in kernel matrices.

## 5. Experiments

### 5.1. Visual feature implementations

In this section, we introduce five low-level visual features which describe different aspects of person images, and can be well crafted to show promising results in person re-identification. To particularly cater for person re-id data sets, these feature descriptors are well manipulated in their implementations with configurations and settings best tuned.

*Color\_hist\_LAB patterns.* For color patterns, we extract color features using 32-bins histograms at three different scale factors (0.5, 0.75 and 1) over three different channels: L, A and B. Finally, each histogram feature is normalized with the  $\ell_2$ -norm and concatenated to form the final feature descriptor vector with length 4032.

*LBP/RGB patterns.* Local Binary Pattern (LBP) is another feature descriptor that has received a lot of attention in the literature due to its effectiveness and efficiency [30]. The standard version of 8-neighbours LBP has a radius of 1 and is formed by thresholding the  $3 \times 3$  neighbourhood with the centre pixel's value. To improve the classification accuracy of LBP, we combine LBP histograms with color histograms extracted from the RGB colorspace. Specifically, we rescale pedestrian images to a resolution of  $48 \times 128$  pixels. The LBP and color histograms are then extracted over a set of 7 dense overlapping  $48 \times 32$ -pixels regions with a stepping stride of 16 pixels in the vertical direction. For texture pattern, we extract LBP histograms using 8-neighbours (radius 1 and 2) and 16-neighbours (radius 2 and 3). LBP is applied to grayscale image and each RGB color channel. We adopt an extension of LBP, known as the uniform LBP, which can better filter out noises [42]. The uniform LBP is defined as the binary pattern that contains at most two bit-wise transitions from 0 to 1 or vice versa. For color histogram, we extract color features using 16-bins histograms over six different color channels: R, G, B, Y, Cb and Cr. Finally, each histogram feature is normalized with the  $\ell_1$ -norm and concatenated to form the final feature vector of 9352 dimensions. In this paper, we use the LBP/RGB implementation obtained from [46].

*Hue-Saturation (HS) histogram.* We first re-scale an image to a broader size  $64 \times 128$ , and then build a spatial pyramid by dividing the image into overlapping horizontal stripes of 16 pixels in height. The HS histograms contain  $8 \times 8$  bins, which are computed for the 15 levels of the pyramids (i.e., 8 stripes for the first level plus 7 for the second level of overlapping stripes, where the second level of stripes are created from a sub-image by removing 8 pixels from top, bottom, left, and right of the original in order to remove background interference.). Each feature histogram is normalized with the  $\ell_2$ -norm and we have the vector length to be 960.

*RGB histogram.* RGB is quantized into  $8 \times 8 \times 8$  over R, G, B channels. Like the extraction of HS, RGB histograms are also computed for the 15 levels of the pyramids, and each histogram feature is normalized with the  $\ell_2$ -norm, forming 7680-dim feature descriptor. We illustrate the procedure of extracting HS and RGB histograms in Fig. 2. Horizontal stripes capture information about vertical color distribution in the image, while overlapping stripes maintain color correlation between adjacent stripes in the final descriptor [23]. Overall, the use of HS histogram renders a portion of the descriptor invariant to illumination variations, while the RGB histograms capture more discriminative color information, especially for dark and greyish colors.



*SIFT/LAB patterns.* Scale-invariant feature transform (SIFT) has gained a lot of research attention due to its invariance to scaling, orientation and illumination changes [25]. The descriptor represents occurrences of gradient orientation in each region. In this work, we employ discriminative SIFT extracted from the LAB colorspace. Images of the persons are first rescaled to a resolution of  $48 \times 128$  pixels. SIFT are extracted over a set of 14 dense overlapping  $32 \times 32$ -pixels regions with a stepping stride of 16 pixels in both directions. Specifically, we divide each region into  $4 \times 4$  cells and set the number of orientation bins to 8. As a result, we can obtain the feature vector with length 5376. In this paper, we use the SIFT/LAB implementation obtained from [50].

## 5.2. Experimental settings

*Datasets.* There exist several challenging benchmark data sets for person re-identification. In this experiment, we select four commonly used data sets (iLIDS, 3DPES, PRID2011, VIPeR) and two recently introduced data sets with a large number of individuals (CUHK01 and CUHK03). The iLIDS data set has 119 individuals captured from eight cameras with different viewpoints [53]. The number of images for each individual varies from 2 to 8, i.e., eight cameras are used to capture 119 individuals. The data set consists of large occlusions caused by people and luggages. The 3DPeS data set is designed mainly for people tracking and person re-identification [1]. It contains numerous video sequences taken from a real surveillance environment with eight different surveillance cameras and consists of 192 individuals. The number of images for each individual varies from 2 to 26 images. The Person RE-ID 2011 (PRID2011) data set consists of images extracted from multiple person trajectories recorded from two surveillance static cameras [15]. Camera view A contains 385 individuals, camera view B contains 749 individuals, with 200 of them appearing in both views. Hence, there are 200 person image pairs in the dataset. VIPeR is one of the most popular used data sets for person re-identification [12]. It contains 632 individuals taken from two cameras with arbitrary viewpoints and varying illumination conditions. The CUHK01 data set contains 971 persons captured from two camera views in a campus environment [20]. Camera view A captures the frontal or back view of the individuals while camera view B captures the profile view. Finally, the CUHK03 data set consists of 1360 persons taken from six cameras [21]. The data set consists of manually cropped pedestrian images and images cropped from the pedestrian detector of [8]. Due to the imperfection in the pedestrian detector, which causes some misalignments of cropped images, we use images which are manually annotated by hand.

*Competitors.* We consider the following state-of-the-art as competitors: 1) MidLevel [51]; 2) LADF [22]; 3) SalMatch [49]; 4) KISSME [19]; 5) PCCA [27]; 6) PRDC [52]; 7) eSDC [50]; 8) SDALF [7]; 9) ISR [23]; 10) ITML [5]; 11) LMNN [43]. Each algorithm is tuned to show their best performance.

*Evaluation protocol.* In this paper, we adopt a single-shot experiment setting, similar to [22, 33, 46, 51, 54]. For all data sets

except CUHK03, all the individuals in the data set are randomly divided into two subsets so that the training set and the test set contains half of the available individuals with no overlap on person identities. For data set with two cameras, we randomly select one image of the individual taken from camera view A as the probe image and one image of the same individual taken from camera view B as the gallery image. For multi-camera data sets, two images of the same individual are chosen: one is used as the probe image and the other as the gallery image. For CUHK03, we set the number of individuals in the train/test split to 1260/100 as conducted in [21]. To be more specific, there are 59, 96, 100, 316, 485 and 100 individuals in each of the test split for the iLIDS, 3DPeS, PRID2011, VIPeR, CUHK01 and CUHK03 data sets, respectively. The number of probe images (test phase) is equal to the number of gallery images in all data sets except PRID2011, in which the number of probe images is 100 and the number of test gallery images is 649 (all images from camera view B except the 100 training samples). This procedure is repeated 10 times and the average of cumulative matching characteristic (CMC) curves across 10 partitions is reported. The CMC curve provides a ranking for every image in the gallery with respect to the probe.

*Parameters setting.* For the linear base metric (KISS ML [19]), we apply principal component analysis (PCA) to reduce the dimensionality and remove noise. Without performing PCA, it is computationally infeasible to inverse covariance matrices of both similar and dissimilar pairs as discussed in [19]. For each visual feature, we reduce the feature dimension to 64 dimensional subspaces. For the non-linear base metric (kLFDA [46]), we set the regularization parameter for class scatter matrix to 0.01, i.e., we add a small identity matrix to the class scatter matrix. For all features, we apply the RBF- $\chi^2$  kernel. The kernel parameter is tuned to an appropriate value for each data set. In this experiment, we set the value of  $\sigma^2$  to be the same as the first quantile of all distances [46]. For  $\text{CMC}^{\text{triplet}}$ , we choose the regularization parameter ( $\nu$  in (1)) from  $\{10^3, 10^{3.1}, \dots, 10^4\}$  by cross-validation on the training data. For  $\text{CMC}^{\text{top}}$ , we choose the regularization parameter ( $\nu$  in (7)) from  $\{10^2, 10^{2.1}, \dots, 10^3\}$  by cross-validation on the training data. We set the cutting-plane termination threshold to  $10^{-6}$ . The recall parameter ( $k$  in (6)) is set to be 10 for iLIDS, 3DPeS, PRID2011 and VIPeR and 40 for larger data sets (CUHK01 and CUHK03). Since the success of metric learning algorithms often depends on the choice of good parameters, we train multiple metric learning for each feature. Specifically, for KISS ML, we reduce their feature dimensionality to 32, 48 and 64 dimensions and use all three to learn the weight  $w$  for  $\text{CMC}^{\text{triplet}}$  and  $\text{CMC}^{\text{top}}$ . Similarly, for kFLDA, we set the  $\sigma^2$  to be the same as the 5<sup>th</sup>, the 10<sup>th</sup> and the first quantile of all distances.

## 5.3. Evaluation and analysis

*Feature evaluation.* We investigate the impact of low-level visual features on the recognition performance of person re-identification. Fig. 3 shows the CMC performance of different visual features and their rank-1 recognition rates when trained



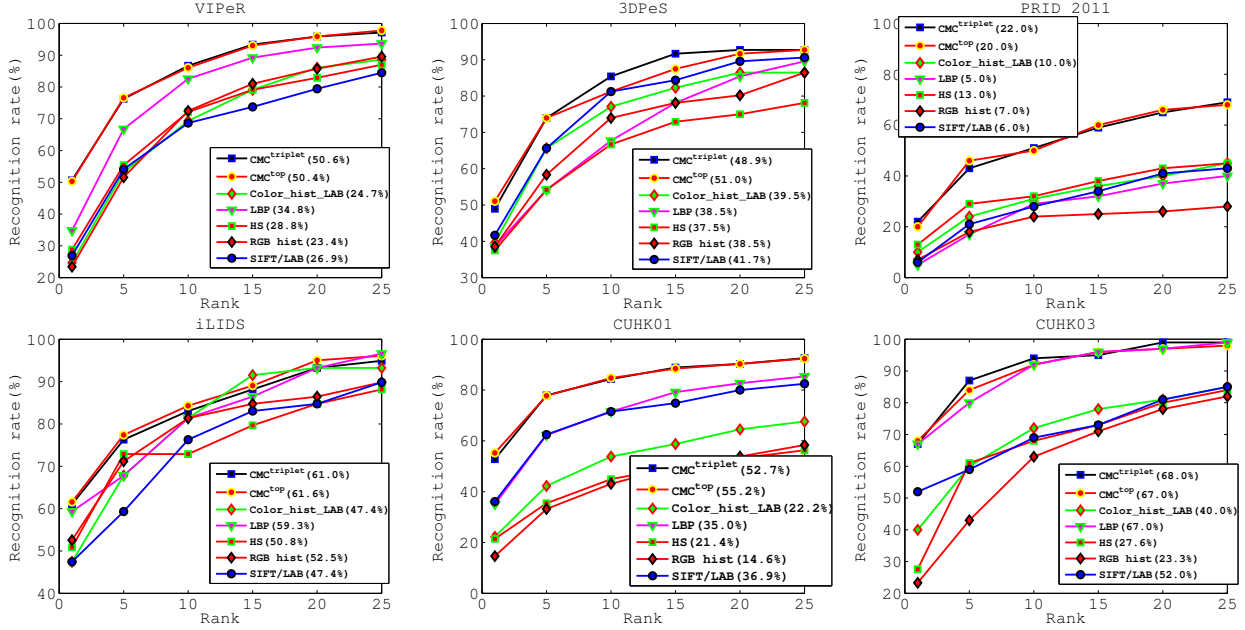


**Figure 3:** Performance comparison of base metrics (non-linear) with different visual features: Color\_hist\_LAB, LBP, HS, RGB histogram, and SIFT/LAB. Rank-1 recognition rates are shown in parentheses. The higher the recognition rate, the better the performance.  $\text{CMC}^{\text{top}}$  represents our ensemble approach which optimizes the CMC score over the top  $k$  returned candidates.  $\text{CMC}^{\text{triplet}}$  represents our ensemble approach which minimizes the number of returned candidates such that the rank- $k$  recognition rate is equal to one.

with the kernel-based LFDA on six benchmark data sets. We have the following observations:

- In VIPeR, iLIDS, and CUHK03 data sets, LBP/RGB and Color\_hist\_LAB are more effective than other features. Since LBP/RGB encodes texture and color features, we suspect the use of color helps improve the overall recognition accuracy of LBP/RGB. In these data sets, a large number of persons wear similar types of clothing but with different color. Therefore, color information becomes an important cue for recognizing two different individuals. In some scenarios where color cue is not reliable because of illuminations, texture helps to identify the same individual.
- In 3DPeS and CUHK01 data sets, SIFT/LAB and LBP/RGB are more effective in recognition. This can be ascribed to the fact that many samples are captured by zoomed/translated cameras (in 3DPeS) or orientation changes (in CUHK01) whilst SIFT/LAB is invariant to scale and orientation.
- In PRID 2011 database, HS becomes predominant feature. This is because this database consist of images captured with little exposure to illuminations in which both color and texture cues become unreliable whilst HS histograms are invariant to illumination changes.

In fact, these person re-id data sets are created with distinct photometric and geometric transformations due to their own lighting conditions and camera settings. In this end, low-level features that are combined properly can be used to characterize the designed features of these data sets. Since our proposed

optimization yields a weight vector for distance functions, it is informative to characterize the nature of different test data sets and the effects of low-level features in recognizing persons are adaptive to these data sets. We show the weight distributions of corresponding features on six benchmarks in Fig. 5. It can be seen that in VIPeR, iLIDS and 3DPeS data sets, the features of color, LBP and SIFT are more effective, thus they are more likely to be assigned larger weight coefficients. In CUHK01 and CUHK03 databases, LBP, SIFT and HS are more helpful to recognize individuals due to the fact that many samples in the two data sets undergo photometric and geometric transforms caused by the change of lighting conditions, viewpoints, and human-pose whereas SIFT and HS are invariant to orientation and illumination changes, respectively. In PRID 2011 data set, HS and color hints (Color\_hist\_LAB and RGB) are predominant features.

We also provide experimental results of *linear metric learning* [19] with different visual features. The CMC curve can be found in Fig. 4. Recall Fig. 3, we observe that: 1) non-linear based kernels perform better than linear metrics on most visual features. A significant performance improvement is found in CUHK03 data set, where we observe a performance improvement from 12.0% to 52.0% for SIFT/LAB features, and an improvement from 27.0% to 67.0% for LBP/RGB features; 2) our method is highly flexible to both linear/non-linear metric learning, and the effects of visual features in recognizing persons are almost the same in using linear or non-linear metric learning.

*Ensemble approach with linear/non-linear metric learning.* We conduct the performance comparison of our approach with two

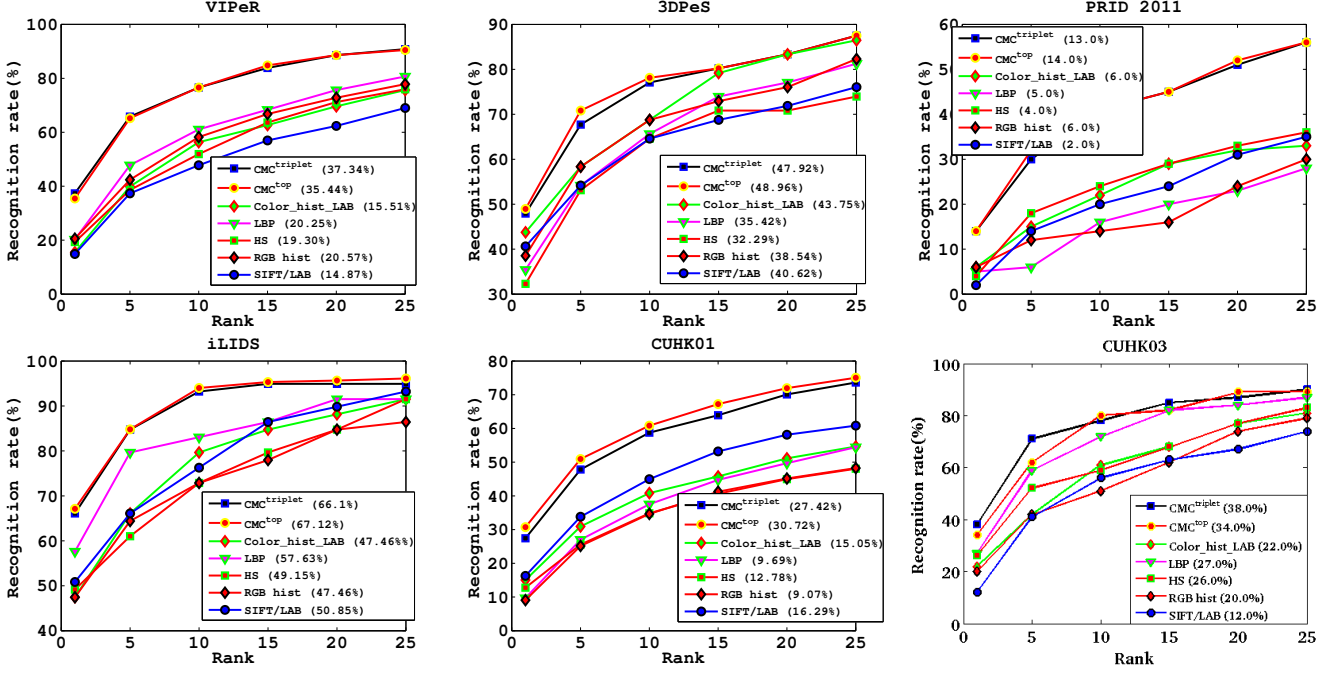


**Figure 4:** Performance comparison of base metrics (linear) with different visual features: Color\_hist\_LAB, LBP, HS, RGB histogram, and SIFT/LAB. Rank-1 recognition rates are shown in parentheses. The higher the recognition rate, the better the performance. CMC<sup>top</sup> represents our ensemble approach which optimizes the CMC score over the top  $k$  returned candidates. CMC<sup>triplet</sup> represents our ensemble approach which minimizes the number of returned candidates such that the rank- $k$  recognition rate is equal to one.

different base metrics: linear metric learning (KISSME) [19] and kernel metric learning (kLFDA) [46]. In this experiment, we use CMC<sup>top</sup> to learn an ensemble. Experimental results are shown in Fig. 6. Two observations can be made from the figure:

- Both approaches perform similarly when the number of train/test individuals is small, e.g., on iLIDS and 3DPeS;
- Non-linear base metrics outperforms linear base metric by a large margin when the number of individuals increase as in CUHK01 and CUHK03 data sets. This is because in KISSME it employs PCA to reduce the dimensionality of data since it requires solving a generalized eigenvalue problem of very large scatter  $d \times d$  matrices where  $d$  denotes the dimensionality of features. However, this dimensionality step, when applied to relatively diverse data set, can result in an undesirable compression of the most discriminative features. In contrast, kLFDA can avoid performing such decomposition, and flexible in choosing the kernel to improve the classification accuracy.

*Performance at different recall values.* Next we compare the performance of CMC<sup>triplet</sup> with CMC<sup>top</sup>. Both algorithms optimize the recognition rate of person re-id but with different objective criteria. Since distance functions of different features have different scales, we normalize the distance between each probe image to all images in the gallery to be between zero and

one. In other words, we set the distance between the probe image and the nearest gallery image to be zero and the distance between the probe image and the furthest gallery image to be one. The matching accuracy is shown in Table 1. We observe that CMC<sup>top</sup> achieves the best recognition rate performance at a small recall value. At a large recall value (rank  $\geq 50$ ), both CMC<sup>top</sup> and CMC<sup>triplet</sup> perform similarly.

#### 5.4. Comparison with state-of-the-art results

Fig. 7 compares our results with other person re-id algorithms on two major benchmark data sets: VIPeR and CUHK01. Our approach outperforms all existing person re-id algorithms. Then we compare our results with the best reported results in the literature, and shown in Table 2. The algorithm proposed in [46] achieves state-of-the-art results on iLIDS and 3DPeS data sets (40.3% and 54.2% recognition rate at rank-1, respectively). Our approach outperform [46] on the iLIDS (61.3%) by a large margin, and achieve a comparable result on 3DPeS (51.1%). Zhao *et al.* propose mid-level filters for person re-identification [51], which achieve state-of-the-art results on the VIPeR and CUHK01 data sets (43.39% and 34.30% recognition rate at rank-1, respectively). Our approach outperforms [51] by achieving a recognition rate of 50.6% and 55.2% on the VIPeR and CUHK01 data sets, respectively.

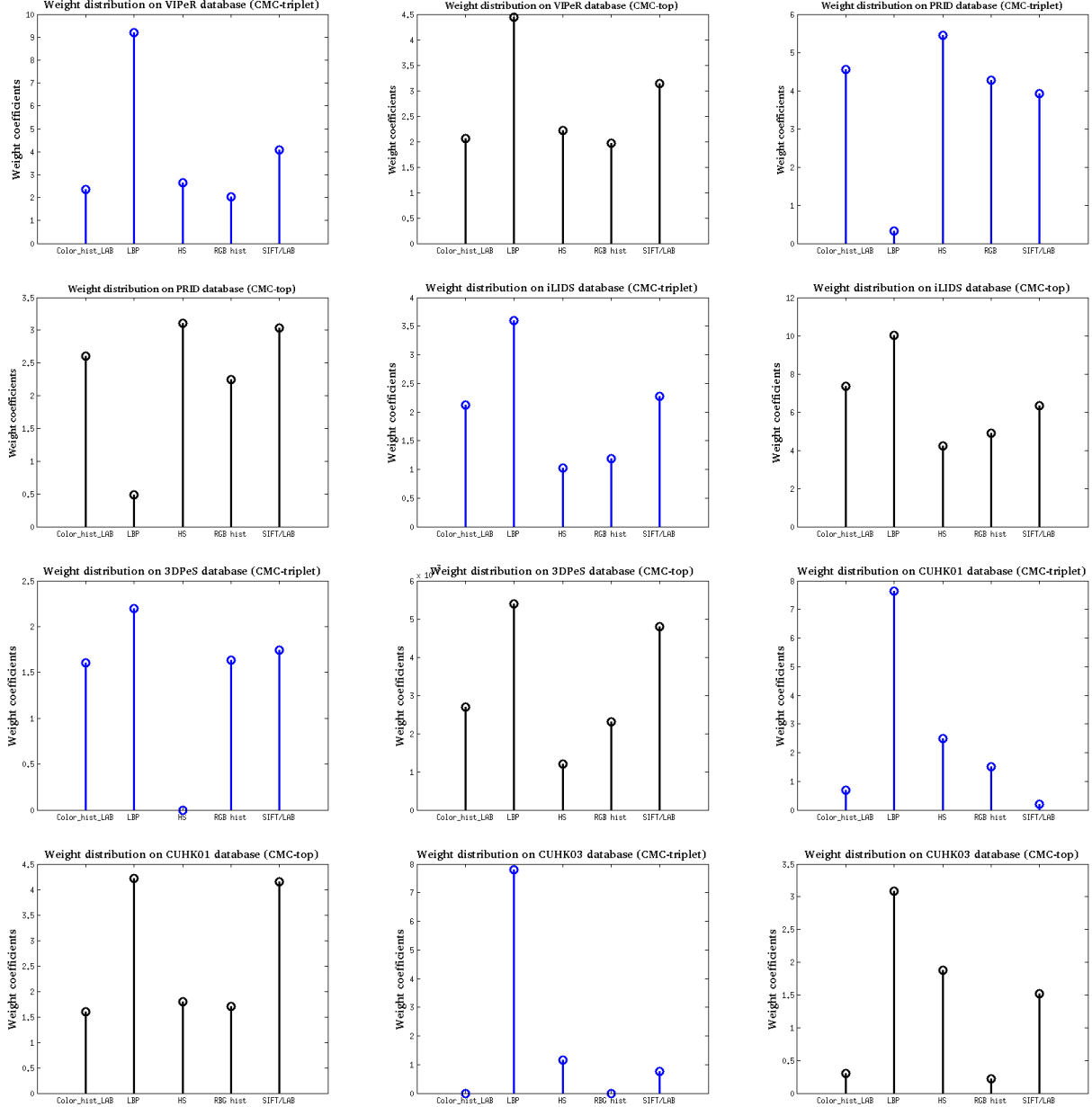


**Figure 5:** Weight distributions on six datasets that can reflect the adaptive effects of low-level features in recognizing individuals.

### 5.5. Comparison with a structured learning-based person re-id [45]

In this section, we compare our ensemble approaches with another structured learning-based method for person re-identification proposed in [45]. The authors of [45] apply the metric learning to rank (MLR) algorithm of [26] with a listwise loss function (mean reciprocal rank) to the person re-identification problem and report their results using Mean Reciprocal Rank (MRR). We train MLR with the MRR loss. For a fair comparison, we concatenate low-level visual features and learn MLR [45] and LMNN [43] on VIPeR data set. We choose the MLR trade-off parameter from  $\{10^{-5}, 10^{-4}, \dots, 10^5\}$ . The rank-1 recognition rate and mean reciprocal rank (MRR) are shown in the Table 3. Our ensemble approach significantly

outperforms both baseline methods under both evaluation criteria. We point out here that the use of structured output to rank person re-id candidates (both our approach and [45]) is not the key contribution that makes our approach outperform all existing methods. In our experiments, we observe that both  $\text{CMC}^{\text{top}}$  and  $\text{CMC}^{\text{triplet}}$  outperform existing methods (see Table 1 and Table 2). These results indicate that even our non-ranking based method ( $\text{CMC}^{\text{triplet}}$ ) already performs better than all existing works; and our ranking based method ( $\text{CMC}^{\text{top}}$ ) further improves the accuracy.

### 5.6. Compatibility to early fusion of features

Concatenating low-level features has been demonstrated to be powerful in person re-id application [51, 50]. Our approaches

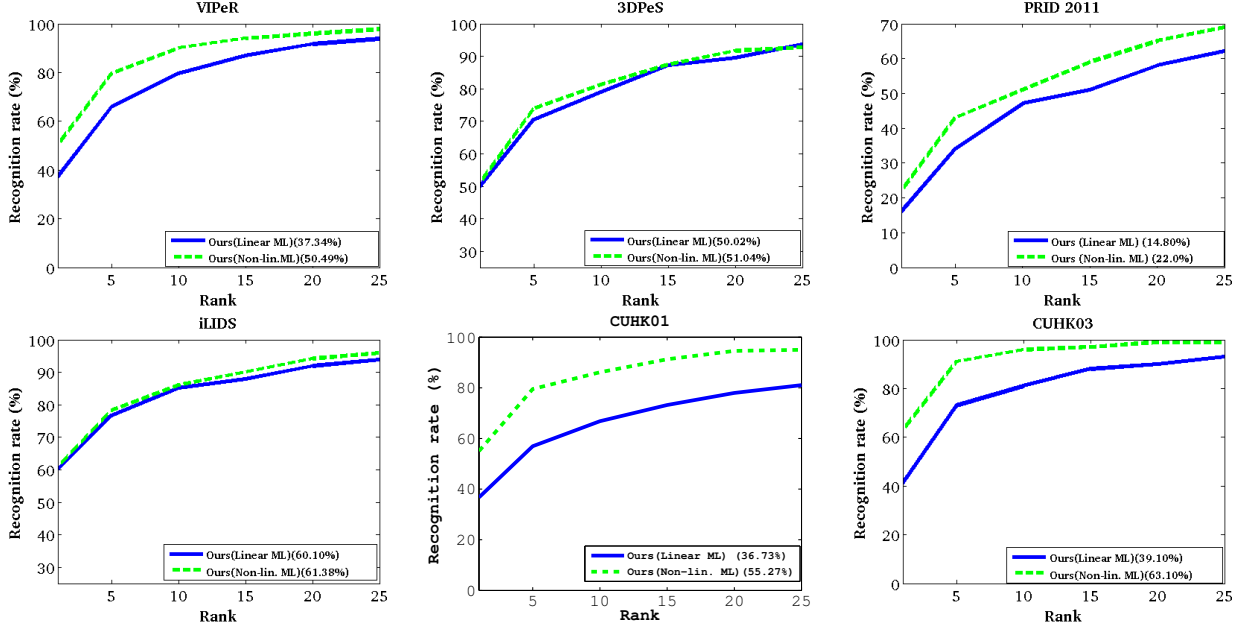


**Figure 6:** Performance comparison of  $\text{CMC}^{\text{top}}$  with two different base metrics: linear base metric (Linear Metric Learning) and non-linear base metric (Non-lin. Metric Learning). On VIPeR, PRID 2011, CUHK01 and CUHK03 data sets, an ensemble of non-linear base metrics significantly outperforms an ensemble of linear base metrics.

Rank	VIPeR			CUHK01			CUHK03		
	Avg.	$\text{CMC}^{\text{triplet}}$	$\text{CMC}^{\text{top}}$	Avg.	$\text{CMC}^{\text{triplet}}$	$\text{CMC}^{\text{top}}$	Avg.	$\text{CMC}^{\text{triplet}}$	$\text{CMC}^{\text{top}}$
1	50.4	50.3	<b>50.6</b>	52.5	53.0	<b>55.2</b>	59.5	67.0	<b>68.1</b>
2	61.0	<b>61.4</b>	<b>61.4</b>	63.5	64.1	<b>64.9</b>	71.9	74.0	<b>77.8</b>
5	76.5	77.3	<b>77.6</b>	77.1	76.7	<b>77.5</b>	86.4	85.8	<b>89.3</b>
10	88.4	88.6	<b>88.9</b>	84.3	<b>84.8</b>	84.5	92.3	92.5	<b>95.3</b>
20	95.9	<b>95.9</b>	<b>95.9</b>	92.1	91.7	<b>92.5</b>	96.9	<b>99.0</b>	<b>97.0</b>
50	99.4	<b>99.7</b>	99.5	97.0	<b>97.1</b>	96.9	99.8	99.7	<b>100.0</b>
100	99.9	<b>100.0</b>	<b>100.0</b>	98.6	<b>98.6</b>	<b>98.6</b>	<b>100.0</b>	<b>100.0</b>	<b>100.0</b>

**Table 1:** Re-id recognition rate (%) at different recall (rank). The best result is shown in boldface. Both  $\text{CMC}^{\text{top}}$  and  $\text{CMC}^{\text{triplet}}$  achieve similar performance when retrieving  $\geq 50$  candidates.

Data set	# Individuals		Prev. best	Ours
	train	test		
iLIDS	59	60	40.3% [46]	<b>61.3%</b>
3DPeS	96	96	<b>54.2%</b> [46]	51.1%
PRID2011	100	100	16.0% [36]	<b>22.0%</b>
VIPeR	316	316	43.4% [51]	<b>50.6%</b>
CUHK01	486	485	34.3% [51]	<b>55.2%</b>
CUHK03	1260	100	20.7% [21]	<b>68.1%</b>

**Table 2:** Rank-1 recognition rate of existing best reported results and our results. The best result is shown in boldface.

**Table 3:** Rank-1 recognition rate and mean reciprocal rank (MRR) of different algorithms. The closer the result to 1, the better the algorithm. The experimental result reported here for MLR+MRR is better than the one reported in [45] as the authors of [45] only use color histogram feature.

Algorithm	Rank-1 rate	MRR
LMNN [43]	24.9%	37.8%
MLR+MRR [45]	26.2%	39.9%
$\text{CMC}^{\text{top}}$ + linear metric	37.3%	47.3%
$\text{CMC}^{\text{top}}$ + non-linear metric	50.6%	60.1%

can be essentially regarded as a late fusion paradigm where base metrics are first learnt from training samples, which are then fed into visual features to seek their individual weights. In this section, we study the compatible property of our method to early fusion of visual features. Since we have five types of

hand-crafted features, hence there are  $\sum_{k=1}^5 C_5^k$  combinatorial strategies in total, as shown in Table 4, where  $\checkmark$  denotes the selection of candidate features in concatenation. For instance,  $F6$  indicates a feature which is formed by concatenating  $F1$  (Color\_hist\_LAB) and  $F2$  (LBP) into a single feature vector.

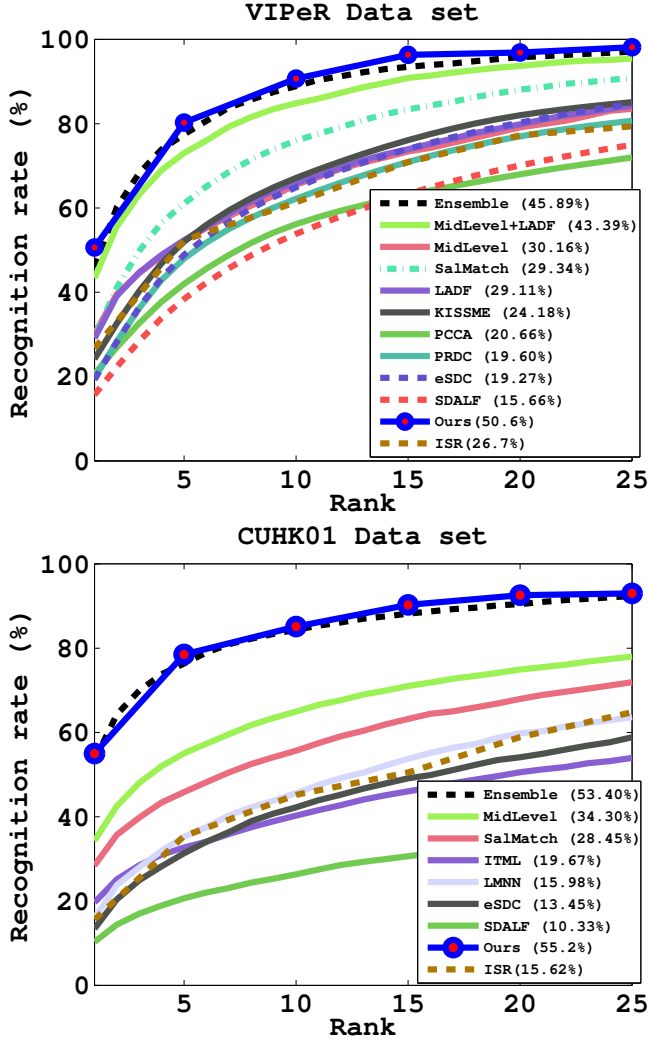


**Figure 7:** CMC performance for VIPeR and CUHK01 data sets. The higher the recognition rate, the better the performance. Our approach outperforms all existing person re-id algorithms.

Our approaches are conducted to learn weights for ensembling these base metrics. Evaluation results are reported in Table 5–7, where kLFDA is employed to perform metric learning. We have the following observations:

- Our ensemble-based approaches consistently outperform any kind of concatenated features in rank- $k$  recognition rates, demonstrating the effectiveness in combining these features with adaptive weights. Simply concatenating features is essentially to assign equally pre-defined weights to their metric, which is not robust enough against complex variations in illumination, pose, viewpoints, camera setting, and background clutter across camera views.
- Incorporating more base metrics is beneficial to our algorithms. In most cases, the increasingly availability of base metrics contribute to either achieve slight improvement in rank- $k$  recognition rate or keep the state-of-the-art re-

sults from Table 2. This demonstrates the robustness of our approaches against feature selection.

- Some low-level features are complementary to each other, and consequently, their concatenations give promising results, e.g., in iLIDS, F22 (concatenation of LBP, HS, and RGB histogram) shows superior performance to other fusion strategies. However, this pre-defined combination is lack of generalization, and only suits to specific data sets, e.g., in 3DPeS, F22 is inferior to F25.

### 5.7. Comparison with metric learning algorithm

We also use the following metric learning algorithms: large scale metric learning from equivalence constraints (KISSME) [19], large margin nearest neighbor (LMNN) [43] and logistic distance metric learning (LDML) [14]. These implementations are publicly available and can be downloaded from authors' websites: KISSME<sup>2</sup>, LMNN<sup>3</sup> and LDML<sup>4</sup>.

#### 5.7.1. Metric learning

We first apply principal component analysis (PCA) to reduce the dimensionality and remove noise. Without performing PCA, it is computationally infeasible to perform distance metric learning on KISSME as discussed in [19]. To ensure a fair comparison, we use the same number of PCA dimensions in all metric learning algorithms. In this experiment, we reduce the feature dimension to 32 and 64 dimensional subspaces. We use the following parameters for three different metric learning algorithms:

**KISSME.** Apart from PCA dimensions, KISSME has two parameters: (a) influence of the similar and dissimilar pairs; (b) the option to enforce the linear mapping matrix ( $M$ ) learned to be positive semi-definite matrix ( $M_+$ ) by back-projecting. In this experiment, we set (a) to the value of 1 and turn on (b). These are the default values as suggested by the authors of [19].

**LMNN.** The LMNN algorithm consists of several parameters. We keep most parameters to be default values as suggested by the authors of [43]. We modify the following parameters: (a) the number of nearest neighbors; (b) fraction of training data to be used as validation set; (c) maximum number of iterations. In this experiment, we set (a) to 1 (there are only two images from two camera views of the same identity, therefore the number of nearest neighbors is 1), (b) to 0 (use all data as the training data), and (c) to 1000 (to speed up the experiment. Note the default is 10000).

**LDML.** This algorithm has three parameters: (a) the number of dimensions of projection space; (b) the number of iterations; (c) the parameter initialization vector. We set all parameters to be the default values [14], i.e., set (a) to be the same as the number of PCA dimensions, set (b) to be 100 and set (c) to be random.

<sup>2</sup><http://lrs.icg.tugraz.at/research/kissme/>

<sup>3</sup><http://www.cse.wustl.edu/~kilian/code/lmnn/lmnn.html>

<sup>4</sup><http://lear.inrialpes.fr/people/guillaumin/code.php>

**Table 4:** The indication table for early fusion strategies of low-level features. Color.hist.LAB (F1), LBP (F2), HS (F3), RGB hist (F4), SIFT/LAB(F5).

	F1	F2	F3	F4	F5		F1	F2	F3	F4	F5
F6	✓	✓				F19	✓		✓	✓	
F7	✓		✓			F20	✓		✓		✓
F8	✓			✓		F21	✓			✓	✓
F9	✓				✓	F22		✓	✓	✓	
F10		✓	✓			F23		✓	✓		✓
F11		✓		✓		F24		✓		✓	✓
F12		✓			✓	F25			✓	✓	✓
F13			✓	✓		F26	✓	✓	✓	✓	
F14			✓		✓	F27	✓	✓	✓		✓
F15				✓	✓	F28	✓	✓		✓	✓
F16	✓	✓	✓			F29	✓		✓	✓	✓
F17	✓	✓		✓		F30		✓	✓	✓	✓
F18	✓	✓			✓	F31	✓	✓	✓	✓	✓

*Experimental results.* We compare rank-1 identification rates of three different metric learning algorithms in Table 8 (The results with 32-dim are shown in parentheses). Our results are averaged over 10 trials of CMC<sup>top</sup> with KISSME as the base metric. The three metric learning algorithms take the concatenation of five low-level features as input while our approach is conducted to learn a set of weights adaptive to these distance functions. We observe that we achieve superior performance to state-of-the-art metric learning methods that combine the same range of feature vectors as input. However the performance of all metric learning algorithms improves as we increase the number of PCA dimensions. Possible reasons that might have caused significant performance differences between our obtained results and baselines of metric learning are: (a) learning weights for distance functions is more adaptive to sample variations in a variety of person re-id databases; (b) optimizing the test criteria directly is beneficial to improving recognition rate.

### 5.8. Approximating kernel learning

As shown in above empirical study, an ensemble of kernel based metrics remarkably outperforms that of liner base metrics, especially in VIPeR, PRID 2011, CUHK01 and CUHK03. Nonetheless, the application of non-linear metric learning is recognized to be limited in the case of large-scale data set such as CUHK03 or even medium-sized data set such as CUHK01 due to the high computational cost in kernel learning. To this end, we resort to approximate kernel learning by using the Nyström method which is able to approximate the full kernel matrix by a low rank matrix with the additional error of  $O(1/m)$  in the generalization performance. Fig. 8 shows the performance of our method with varied number of random samples. Note that for the large data set CUHK03, we restrict the maximum number of random samples to 300 because of the high computational cost. We observe that the approximate counterpart is able to achieve comparable results to the original method with a full kernel matrix. We finally evaluate whether the key assumption of large eigengap holds for these person re-id data

sets. As shown in Fig. 9 (eigenvalues are in logarithm scale), it can be seen that the eigenvalues drop very quickly as the rank increases, yielding a dramatic gap between the top eigenvalues and the remaining ones.

## 6. Conclusion

In this paper, we have presented two effective structured learning based approaches for person re-id by combining multiple low-level visual features into a single framework. The approaches are generalized and adaptive to different person re-id datasets by automatically discovering the effects of visual features in recognizing persons. Extensive experimental studies demonstrate the our approaches advance the state-of-the-art results by a significant margin. Our framework is practical to real-world applications since the performance can be concentrated in the range of most practical importance. Moreover our approaches are flexible and can be applied to any metric learning algorithms. Future works include incorporating depth from a single monocular image [24], integrating person re-id with person detector [32] and improving multiple target tracking of [28] with the proposed approaches.

## References

- [1] Baltieri, D., Vezzani, R., Cucchiara, R., 2011. 3DPes: 3D people dataset for surveillance and forensics. In: Proc. of Int'l. Workshop on Mult. Acc. to 3D Human Objs.
- [2] Bazzani, L., Cristani, M., Perina, A., Murino, V., 2012. Multiple-shot person re-identification by chromatic and epitomic analyses. Patt. Recogn. 33 (7), 898–903.
- [3] Cheng, D. S., Cristani, M., Stoppa, M., Bazzani, L., Murino, V., 2011. Custom pictorial structures for re-identification. In: Proc. British Mach. Vis. Conf.
- [4] Chopra, S., Hadsell, R., LeCun, Y., 2005. Learning a similarity metric discriminatively, with application to face verification. In: Proc. IEEE Conf. Comp. Vis. Patt. Recogn.
- [5] Davis, J. V., Kulis, B., Jain, P., Sra, S., Dhillon, I. S., 2007. Information-theoretic metric learning. In: Proc. Int. Conf. Mach. Learn.



**Table 5:** Rank-1, Rank-5, and Rank-10 recognition rate of various early fusion strategies over VIPeR and iLIDS databases.

Feature	VIPeR			iLIDS		
	CMC(1)	CMC(5)	CMC(10)	CMC(1)	CMC(5)	CMC(10)
F1	22.4%	50.6%	67.7%	47.4%	67.7%	81.3%
F2	35.4%	63.6%	77.2%	59.3%	67.7%	81.3%
F3	23.7%	54.4%	70.2%	50.8%	72.8%	72.8%
F4	26.2%	53.4%	69.3%	52.5%	71.1%	81.3%
F5	27.8%	54.7%	68.6%	47.4%	59.3%	76.2%
F6	31.0%	63.2%	78.1%	49.1%	71.1%	83.0%
F7	29.1%	61.0%	76.8%	50.8%	69.4%	79.6%
F8	25.6%	60.7%	76.5%	54.2%	69.4%	79.6%
F9	34.4%	68.6%	80.0%	54.2%	71.1%	74.5%
F10	39.5%	69.6%	82.9%	60.7%	77.9%	84.7%
F11	38.6%	70.2%	84.8%	59.3%	72.8%	86.4%
F12	35.7%	68.9%	82.5%	55.9%	66.1%	77.9%
F13	34.1%	68.3%	82.2%	52.5%	71.1%	74.5%
F14	38.9%	68.6%	81.3%	50.8%	69.4%	79.6%
F15	37.6%	71.2%	83.5%	50.8%	62.7%	79.6%
F16	34.8%	68.9%	81.9%	54.2%	72.8%	84.7%
F17	31.6%	70.2%	82.2%	54.2%	71.1%	83.0%
F18	38.9%	72.1%	84.4%	55.9%	71.1%	79.6%
F19	31.9%	66.4%	81.6%	57.6%	71.2%	83.0%
F20	37.3%	73.1%	81.6%	57.6%	71.1%	76.2%
F21	35.7%	71.2%	82.9%	55.9%	71.1%	76.2%
F22	40.1%	75.3%	86.0%	60.7%	74.5%	83.0%
F23	40.8%	74.0%	84.4%	59.3%	67.7%	83.0%
F24	43.3%	75.3%	85.4%	54.2%	66.1%	79.6%
F25	41.4%	74.3%	84.8%	54.2%	72.8%	76.2%
F26	34.1%	72.1%	84.4%	57.6%	71.2%	84.7%
F27	40.1%	75.6%	86.0%	57.6%	72.8%	79.6%
F28	39.2%	73.4%	86.0%	54.2%	72.8%	77.9%
F29	38.9%	74.0%	84.8%	55.9%	71.1%	76.2%
F30	45.8%	75.9%	88.2%	55.9%	69.4%	83.0%
F31	41.7%	75.6%	87.0%	57.6%	72.8%	79.6%
CMC <sup>top</sup>	<b>47.1%</b>	<b>79.7%</b>	<b>88.6%</b>	<b>61.0%</b>	<b>76.3%</b>	<b>86.4%</b>
CMC <sup>triplet</sup>	<b>47.7%</b>	<b>79.1%</b>	<b>88.9%</b>	<b>61.3%</b>	<b>77.1%</b>	<b>86.7%</b>

- [6] Drineas, P., Mahoney, M. W., 2005. On the system for approximating a gram matrix for improved kernel-based learning. *J. Mach. Learn. Res.* 6, 2153–2175.
- [7] Farenzena, M., Bazzani, L., Perina, A., Murino, V., Cristani, M., 2010. Person re-identification by symmetry-driven accumulation of local features. In: *Proc. IEEE Conf. Comp. Vis. Patt. Recogn.*
- [8] Felzenszwalb, P., Girshick, R., McAllester, D., Ramanan, D., 2010. Object detection with discriminatively trained part based models. *IEEE Trans. Pattern Anal. Mach. Intell.* 32 (9), 1627–1645.
- [9] Frome, A., Singer, Y., Fei, S., Malik, J., 2007. Learning globally-consistent local distance functions for shape-based image retrieval and classification. In: *Proc. IEEE Int. Conf. Comp. Vis.*
- [10] Gheissari, N., Sebastian, T. B., Hartley, R., 2006. Person reidentification using spatiotemporal appearance. In: *Proc. IEEE Conf. Comp. Vis. Patt. Recogn.*
- [11] Gong, S., Cristani, M., Yan, S., Loy, C. C., 2014. *Person Re-Identification*. Springer.
- [12] Gray, D., Brennan, S., Tao, H., 2007. Evaluating appearance models for recognition, reacquisition, and tracking. In: *Proc. Int'l. Workshop on Perf. Eval. of Track. and Surv'l.*
- [13] Gray, D., Tao, H., 2008. Viewpoint invariant pedestrian recognition with an ensemble of localized features. In: *Proc. Eur. Conf. Comp. Vis.*
- [14] Guillaumin, M., Verbeek, J., Schmid, C., 2009. Is that you? metric learning approaches for face identification. In: *Proc. IEEE Int. Conf. Comp. Vis.*
- [15] Hirzer, M., Belezni, C., Roth, P. M., Bischof, H., 2011. Person re-identification by descriptive and discriminative classification. In: *Proc. Scandinavian Conf. on Image Anal.*
- [16] Hirzer, M., Roth, P., Bischof, H., 2012. Person re-identification by efficient imposter-based metric learning. In: *Proc. Int'l. Conf. on Adv. Vid. and Sig. Surveillance.*
- [17] Joachims, T., 2005. A support vector method for multivariate performance measures. In: *Proc. Int. Conf. Mach. Learn.*
- [18] Kédem, D., Tyree, S., Sha, F., Lanckriet, G. R., Weinberger, K. Q., 2012. Non-linear metric learning. In: *Proc. Adv. Neural Inf. Process. Syst.*
- [19] Kostinger, M., Hirzer, M., Wohlhart, P., Roth, P. M., Bischof, H., 2012. Large scale metric learning from equivalence constraints. In: *Proc. IEEE Conf. Comp. Vis. Patt. Recogn.*
- [20] Li, W., Zhao, R., Wang, X., 2012. Human reidentification with transferred metric learning. In: *Proc. Asian Conf. Comp. Vis.*
- [21] Li, W., Zhao, R., Xiao, T., Wang, X., 2014. Deepreid: Deep filter pairing neural network for person re-identification. In: *Proc. IEEE Conf. Comp. Vis. Patt. Recogn.*
- [22] Li, Z., Chang, S., Liang, F., Huang, T. S., Cao, L., Smith, J., 2013. Learn-



**Table 6:** Rank-1, Rank-5, and Rank-10 recognition rate of various early fusion strategies over PRID2011 and 3DPeS databases.

Feature	PRID 2011			3DPeS		
	CMC(1)	CMC(5)	CMC(10)	CMC(1)	CMC(5)	CMC(10)
F1	10.1%	24.0%	31.0%	39.5%	65.6%	77.1%
F2	5.0%	17.0%	29.0%	38.5%	54.1%	67.7%
F3	13.0%	29.0%	32.0%	37.5%	54.1%	66.7%
F4	7.0%	18.0%	24.0%	38.5%	58.3%	73.9%
F5	6.0%	21.0%	28.0%	41.6%	65.6%	81.2%
F6	10.0%	28.0%	36.0%	40.6%	68.7%	76.0%
F7	11.0%	28.0%	35.0%	43.7%	67.7%	78.1%
F8	11.0%	28.0%	33.0%	39.5%	65.6%	79.1%
F9	9.0%	29.0%	38.0%	48.9%	71.8%	81.2%
F10	11.1%	24.0%	34.0%	40.6%	59.3%	72.9%
F11	8.0%	17.0%	30.0%	38.5%	56.2%	73.9%
F12	7.0%	22.0%	35.0%	42.7%	70.8%	84.3%
F13	15.0%	33.0%	36.0%	38.5%	64.5%	72.9%
F14	7.0%	21.0%	33.0%	48.9%	73.9%	80.2%
F15	10.0%	23.0%	32.0%	48.9%	76.0%	84.4%
F16	14.0%	28.0%	35.0%	44.7%	68.7%	78.1%
F17	9.0%	29.0%	36.0%	43.7%	67.7%	75.0%
F18	11.0%	31.0%	35.0%	44.7%	71.8%	82.2%
F19	14.0%	33.0%	39.0%	40.6%	64.5%	76.0%
F20	9.0%	32.0%	41.0%	47.9%	70.8%	79.1%
F21	9.0%	28.0%	39.0%	47.9%	72.9%	81.2%
F22	13.0%	26.0%	37.0%	39.5%	60.4%	77.0%
F23	11.0%	24.0%	34.0%	46.8%	77.0%	81.2%
F24	11.0%	25.0%	37.0%	45.8%	75.0%	82.2%
F25	8.0%	21.0%	32.0%	51.0%	73.9%	80.2%
F26	13.0%	30.0%	37.0%	43.7%	68.7%	77.0%
F27	14.0%	30.0%	39.0%	46.8%	70.8%	81.2%
F28	10.0%	31.0%	36.0%	46.8%	75.0%	82.2%
F29	14.0%	32.0%	40.0%	48.9%	70.8%	80.2%
F30	14.0%	27.0%	33.0%	46.8%	72.9%	81.2%
F31	14.0%	28.0%	37.0%	46.8%	69.7%	82.2%
CMC <sup>top</sup>	<b>21.0%</b>	<b>41.0%</b>	<b>49.0%</b>	<b>50.0%</b>	<b>79.1%</b>	<b>85.4%</b>
CMC <sup>triplet</sup>	<b>20.0%</b>	<b>42.0%</b>	<b>50.0%</b>	<b>47.9%</b>	<b>72.9%</b>	<b>83.2%</b>

- ing locally-adaptive decision functions for person verification. In: Proc. IEEE Conf. Comp. Vis. Patt. Recogn.
- [23] Lisanti, G., Masi, I., Andrew D. Bagdanov, A. D. B., 2015. Person re-identification by iterative re-weighted sparse ranking. IEEE Trans. Pattern Anal. Mach. Intell. PP (99), 1.
- [24] Liu, F., Shen, C., Lin, G., 2015. Deep convolutional neural fields for depth estimation from a single image. In: Proc. IEEE Conf. Comp. Vis. Patt. Recogn.
- [25] Lowe, D. G., 2004. Distinctive image features from scale-invariant keypoints. Int. J. Comp. Vis. 60 (2), 91–110.
- [26] McFee, B., Lanckriet, G. R. G., 2010. Metric learning to rank. In: Proc. Int. Conf. Mach. Learn.
- [27] Mignon, A., Jurie, F., 2012. Pcca: a new approach for distance learning from sparse pairwise constraints. In: Proc. IEEE Conf. Comp. Vis. Patt. Recogn. pp. 2666–2672.
- [28] Milan, A., Roth, S., Schindler, K., 2014. Continuous energy minimization for multitarget tracking. IEEE Trans. Pattern Anal. Mach. Intell. 36 (1), 58–72.
- [29] Narasimhan, H., Agarwal, S., 2013. A structural svm based approach for optimizing partial auc. In: Proc. Int. Conf. Mach. Learn.
- [30] Ojala, T., Pietikainen, M., Maenpaa, T., 2002. Multiresolution gray-scale and rotation invariant texture classification with local binary patterns. IEEE Trans. Pattern Anal. Mach. Intell. 24 (7), 971–987.
- [31] Paisitkriangkrai, S., Shen, C., van den Hengel, A., 2015. Learning to rank in person re-identification with metric ensembles. In: Proc. IEEE Conf. Comp. Vis. Patt. Recogn. Boston, USA.
- [32] Paisitkriangkrai, S., Shen, C., Zhang, J., 2008. Fast pedestrian detection using a cascade of boosted covariance features. IEEE Trans. Circuits Syst. Video Technol. 18 (8), 1140–1151.
- [33] Pedagadi, S., Orwell, J., Velastin, S., Boghossian, B., 2013. Local fisher discriminant analysis for pedestrian re-identification. In: Proc. IEEE Conf. Comp. Vis. Patt. Recogn.
- [34] Prosser, B., Zheng, W. S., Gong, S., Xiang, T., Mary, Q., 2010. Person re-identification by support vector ranking. In: Proc. British Mach. Vis. Conf.
- [35] Rahimi, A., Recht, B., 2007. Random features for large-scale kernel machines. In: Proc. Adv. Neural Inf. Process. Syst. pp. 1177–1184.
- [36] Roth, P. M., Hirzer, M., Köstinger, M., Belezni, C., Bischof, H., 2014. Mahalanobis distance learning for person re-identification. In: Person Re-Identification. Springer, pp. 247–267.
- [37] Schultz, M., Joachims, T., 2004. Learning a distance metric from relative comparisons. In: Proc. Adv. Neural Inf. Process. Syst.
- [38] Schwartz, W., Davis, L., 2009. Learning discriminative appearance-based models using partial least squares. In: Proc. of SIBGRAPI.

**Table 7:** Rank-1, Rank-5, and Rank-10 recognition rate of various early fusion strategies over CUHK01 and CUHK03 databases.

Feature	CUHK01			CUHK03		
	CMC(1)	CMC(5)	CMC(10)	CMC(1)	CMC(5)	CMC(10)
F1	18.7%	40.0%	51.9%	30.0%	60.0%	72.0%
F2	33.8%	59.3%	70.5%	60.0%	84.0%	92.0%
F3	21.0%	37.9%	47.4%	27.0%	61.0%	68.0%
F4	14.6%	30.9%	40.8%	23.0%	43.0%	63.0%
F5	36.9%	58.9%	68.4%	27.0%	55.0%	65.0%
F6	25.5%	54.6%	67.2%	53.0%	78.0%	86.0%
F7	24.7%	49.2%	61.8%	47.0%	73.0%	82.0%
F8	25.3%	50.7%	60.2%	39.0%	68.0%	76.0%
F9	36.9%	63.1%	75.4%	36.0%	66.0%	78.0%
F10	39.2%	61.4%	71.3%	52.0%	83.0%	89.0%
F11	34.0%	57.1%	69.4%	51.0%	85.0%	92.0%
F12	45.3%	72.1%	81.4%	47.0%	77.0%	85.0%
F13	27.8%	49.4%	58.2%	37.0%	71.0%	82.0%
F14	41.2%	63.9%	74.0%	38.0%	68.0%	81.0%
F15	42.2%	68.6%	76.1%	37.0%	64.0%	82.0%
F16	32.1%	58.7%	71.9%	55.0%	84.0%	88.0%
F17	31.5%	60.2%	70.7%	52.0%	83.0%	87.0%
F18	42.8%	69.9%	81.4%	46.0%	78.0%	86.0%
F19	28.6%	54.0%	66.2%	45.0%	75.0%	85.0%
F20	41.0%	66.8%	77.5%	47.0%	76.0%	85.0%
F21	39.1%	67.8%	77.1%	40.0%	72.0%	84.0%
F22	37.1%	63.3%	72.8%	59.0%	84.0%	92.0%
F23	49.9%	74.0%	81.8%	52.0%	83.0%	90.0%
F24	47.8%	75.2%	81.0%	50.0%	80.0%	91.0%
F25	45.3%	70.3%	77.7%	42.0%	74.0%	86.0%
F26	34.0%	63.7%	72.5%	60.0%	83.0%	90.0%
F27	46.4%	72.1%	80.8%	55.0%	82.0%	91.0%
F28	44.7%	71.9%	81.4%	52.0%	82.0%	89.0%
F29	42.0%	68.8%	78.1%	51.0%	78.0%	88.0%
F30	49.2%	75.9%	81.8%	54.0%	85.0%	92.0%
F31	46.5%	72.7%	80.6%	55.0%	84.0%	90.0%
CMC <sup>top</sup>	<b>57.1%</b>	<b>76.9%</b>	<b>84.9%</b>	<b>68.0%</b>	<b>86.0%</b>	<b>93.0%</b>
CMC <sup>triplet</sup>	<b>57.5%</b>	<b>77.7%</b>	<b>84.3%</b>	<b>69.0%</b>	<b>87.0%</b>	<b>92.0%</b>

Algorithm	VIPeR	iLIDS	CUHK01
KISSME (32)	34.81%(28.48%)	53.33%(50.00%)	25.51%(19.34%)
LMNN (32)	28.21%(24.72%)	42.97%(39.81%)	24.03%(18.74%)
LDML (32)	27.84%(24.05%)	42.36%(38.03%)	23.87%(18.11%)
CMC <sup>top</sup> (32)	37.34% (33.22%)	60.10% (54.06%)	36.73% (26.36%)

**Table 8:** Comparison with different metric learning algorithms against varied PCA dimensions.

- [39] Shawe-Taylor, J., Cristianini, N., 2004. Kernel Methods for Pattern Analysis. Cambridge University Press.
- [40] Teo, C. H., Smola, A., Vishwanathan, S. V. N., Le, Q. V., 2007. A scalable modular convex solver for regularized risk minimization. In: Proc. of Int. Conf. on Knowl. Disc. and Data Mining.
- [41] Wang, X., Doretto, G., Sebastian, T., Rittscher, J., Tu, P., 2007. Shape and appearance context modeling. In: Proc. IEEE Int. Conf. Comp. Vis.
- [42] Wang, X., Han, T. X., Yan, S., 2009. An HOG-LBP human detector with partial occlusion handling. In: Proc. IEEE Int. Conf. Comp. Vis.
- [43] Weinberger, K., Blitzer, J., Saul, L., 2006. Distance metric learning for large margin nearest neighbor classification. In: NIPS.
- [44] Weinberger, K. Q., Saul, L. K., 2008. Fast solvers and efficient implemen-

- tations for distance metric learning. In: ICML.
- [45] Wu, Y., Mukunoki, M., Funatomi, T., Minoh, M., Lao, S., 2011. Optimizing mean reciprocal rank for person re-identification. In: Advanced Video and Signal-Based Surveillance.
- [46] Xiong, F., Gou, M., Camps, O., Szaier, M., 2014. Person re-identification using kernel-based metric learning methods. In: Proc. Eur. Conf. Comp. Vis.
- [47] Yang, L., Jin, R., 2006. Distance metric learning: A comprehensive survey. Michigan State University 2.
- [48] Yang, T., Li, Y.-F., Mahdavi, M., Jin, R., Zhou, Z.-H., 2012. Nyström method vs random fourier features: a theoretical and empirical comparison. In: Proc. Adv. Neural Inf. Process. Syst.
- [49] Zhao, R., Ouyang, W., Wang, X., 2013. Person re-identification by salience matching. In: Proc. IEEE Int. Conf. Comp. Vis.
- [50] Zhao, R., Ouyang, W., Wang, X., 2013. Unsupervised salience learning for person re-identification. In: Proc. IEEE Conf. Comp. Vis. Patt. Recogn.
- [51] Zhao, R., Ouyang, W., Wang, X., 2014. Learning mid-level filters for person re-identification. In: Proc. IEEE Conf. Comp. Vis. Patt. Recogn.
- [52] Zheng, W., Gong, S., Xiang, T., 2013. Re-identification by relative distance comparison. IEEE Trans. Pattern Anal. Mach. Intell. 35 (653-668), 3.

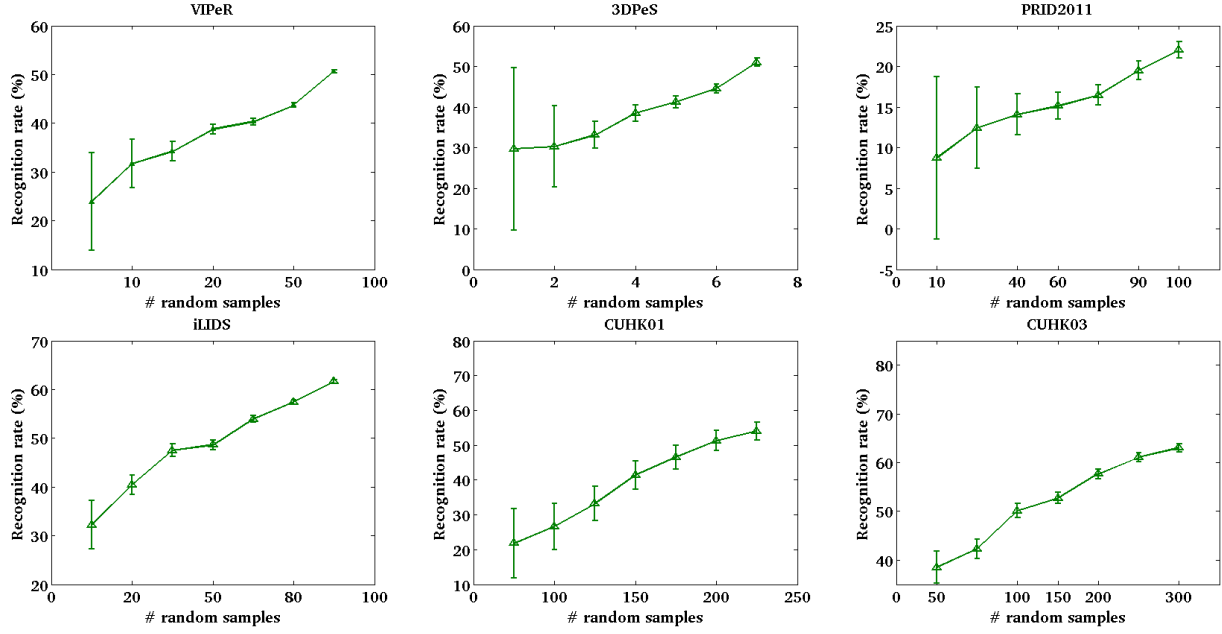


**Figure 8:** Approximate kernel learning by using the Nyström method. The recognition rate at rank-1 of CMC<sup>top</sup> is reported (with std.) against varied number of random samples.

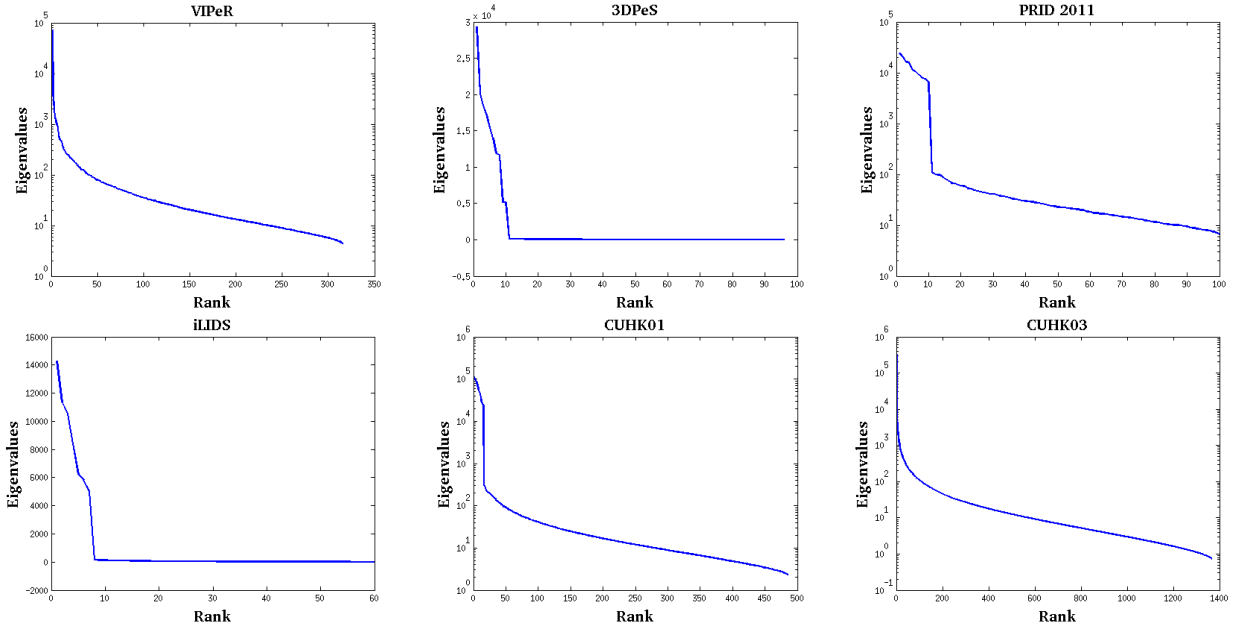


**Figure 9:** The eigenvalue distributions of kernel matrices.

- [53] Zheng, W.-S., Gong, S., Xiang, T., 2009. Associating groups of people. In: Proc. British Mach. Vis. Conf.
- [54] Zheng, W.-S., Gong, S., Xiang, T., 2011. Person re-identification by probabilistic relative distance comparison. In: Proc. IEEE Conf. Comp. Vis. Patt. Recogn.